ANL/GTRI/TM-14/7

RHF RELAP5 Model and Preliminary Loss-Of-Offsite-Power Simulation Results for LEU Conversion

Nuclear Engineering Division

About Argonne National Laboratory
Argonne is a U.S. Department of Energy laboratory managed by UChicago Argonne, LLC under contract DE-AC02-06CH11357. The Laboratory's main facility is outside Chicago, at 9700 South Cass Avenue, Argonne, Illinois 60439. For information about Argonne and its pioneering science and technology programs, see www.anl.gov.

DOCUMENT AVAILABILITY

Online Access: U.S. Department of Energy (DOE) reports produced after 1991 and a growing number of pre-1991 documents are available free via DOE's SciTech Connect (http://www.osti.gov/scitech/)

Reports not in digital format may be purchased by the public from the National Technical Information Service (NTIS):
U.S. Department of Commerce
National Technical Information Service
5301 Shawnee Rd
Alexandria, VA 22312
www.ntis.gov
Phone: (800) 553-NTIS (6847) or (703) 605-6000
Fax: (703) 605-6900
Email: **orders@ntis.gov**

Reports not in digital format are available to DOE and DOE contractors from the Office of Scientific and Technical Information (OSTI):
U.S. Department of Energy
Office of Scientific and Technical Information
P.O. Box 62
Oak Ridge, TN 37831-0062
www.osti.gov
Phone: (865) 576-8401
Fax: (865) 576-5728
Email: **reports@osti.gov**

Disclaimer
This report was prepared as an account of work sponsored by an agency of the United States Government. Neither the United States Government nor any agency thereof, nor UChicago Argonne, LLC, nor any of their employees or officers, makes any warranty, express or implied, or assumes any legal liability or responsibility for the accuracy, completeness, or usefulness of any information, apparatus, product, or process disclosed, or represents that its use would not infringe privately owned rights. Reference herein to any specific commercial product, process, or service by trade name, trademark, manufacturer, or otherwise, does not necessarily constitute or imply its endorsement, recommendation, or favoring by the United States Government or any agency thereof. The views and opinions of document authors expressed herein do not necessarily state or reflect those of the United States Government or any agency thereof, Argonne National Laboratory, or UChicago Argonne, LLC.

ANL/GTRI/TM-14/7

RHF RELAP5 Model and Preliminary Loss-Of-Offsite-Power Simulation Results for LEU Conversion

prepared by

J.R. Licht[1], A. Bergeron[1] and B. Dionne[1]
[1]Nuclear Engineering Division, Argonne National Laboratory, Argonne, IL 60439

and

F. Thomas[2]
[2]RHF Reactor Department, Institut Laue-Langevin (ILL)

August, 2014

This work is sponsored by the

U.S. Department of Energy, National Nuclear Safety Administration NNSA,

Office of Global Threat Reduction (NA-21)

(This page intentionally left blank)

Table of Contents

1. Introduction 5
1.1. Scope 6
2. RELAP5 Model Description 6
2.1. General Considerations 6
2.1.1. RELAP5 version 6
2.1.2. Solution method 6
2.1.3. Coolant volumes 7
2.1.4. Heat structures 8
2.1.5. Materials 8
2.2. Model Overview 8
2.3. Primary Loop (Blue) 9
2.3.1. Measurement locations 10
2.3.2. Heat structures 10
2.3.3. Minor loss coefficients in pipes 10
2.3.4. Primary pump 11
2.3.5. Primary heat exchangers 14
2.4. CRAB Loop (Red) 16
2.4.1. Heat structures 16
2.4.2. Minor loss coefficients 16
2.4.3. Loss of flow 16
2.5. Anti-Syphon Line (Green) 17
2.5.1. Heat structures 17
2.5.2. Minor loss coefficients 17
2.6. Pressurizer (Purple) 17
2.6.1. Heat structures 18
2.6.2. Minor loss coefficients 18
2.6.3. Loss of flow 18
2.7. Natural circulation (Orange) 20
2.7.1. Heat structures 20
2.7.2. Valves 20
2.7.3. Minor loss coefficients 22

2.8. RHF Reactor Vessel 23
2.8.1. Control rod 24
2.8.2. Fuel element 27
2.8.3. Reflector 29
2.8.4. Reactor power 32
2.9. Normal Operation at Zero Power 37
2.10. Previous Known Issues and Resolutions 38
3. Preliminary Loss-of-Offsite-Power Simulations 42
4. Summary and Conclusions 56
5. Future Work 57
References 58
Appendix A: Tees A1
Appendix B: Supporting Analyses for RELAP5 Core Model Discretization B1

1. Introduction

The US Government Highly Enriched Uranium (HEU) minimization effort is led by the National Nuclear Security Administration (NNSA) through the Global Threat Reduction Initiative (GTRI). The program includes the development of advanced Low Enriched Uranium (LEU) fuels, design and safety analyses for research reactor conversion, and technology development for medical isotope production with LEU. This effort has resulted in the successful conversion of many research reactors around the world from HEU to LEU fuel. As part of this initiative, the conversion of the Institut Laue-Langevin (ILL) High Flux Reactor (RHF) was intensified in 2007.

RHF, located in Grenoble France, is a 58.3 MWt tank-in-pool type research reactor dedicated to fundamental science (Figure 1). The core is located inside a heavy water filled tank at the bottom of a light water pool. It consists of a single fuel element comprised of 280 involute curved plates welded to two concentric aluminum tubes. Reactor control is provided by a centrally located control rod. The inlet temperature is ~30°C with a flow rate of 2400 m^3/hr; this flow splits to separately cool the fuel element (primary loop) and control rod (CRAB loop). Each loop has its own heat exchangers and pumps. Three sets of natural circulation lines are available for long term cooling of the core following an accident.

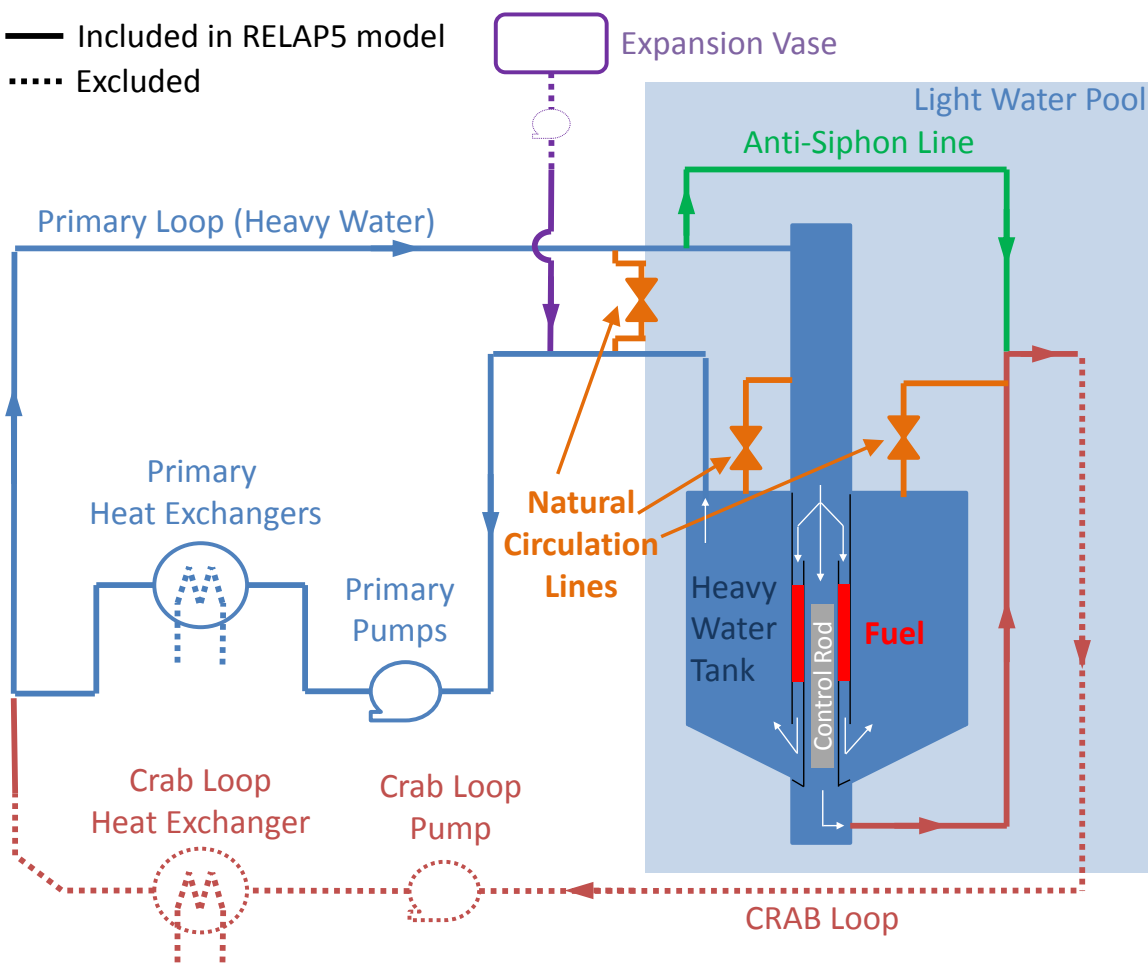

Figure 1 Conceptual drawing of RHF.

1.1. Scope

The purpose of this document is to describe the current state of the RELAP5 model for RHF and provide an update to the key information required to complete, for example, simulations for a loss of offsite power (LOOP) accident. A previous status report identified a list of 22 items to be resolved in order to complete the RELAP5 model [1]. Most of these items have been resolved by ANL and the RHF team. Enough information was available to perform preliminary safety analyses and define the key items that are still required.

Section 2 of this document describes the RELAP5 model of RHF. The model was largely based on the piping system extracted from the RHF CATHARE model [2] and component descriptions provided in the RHF Safety Analysis Report (SAR) [3]. Calibrations of the various components of the RELAP5 model were based primarily on information from the SAR and previous thermal-hydraulic analyses [4]. Results for steady-state conditions at zero power and the calibration for pump coast down are also included. The calibration against reactor loss-of-flow experimental data [5] was performed to obtain the torque friction values for the pumps as well as the time dependent behavior of the natural circulation valves. The final part of this section briefly summarizes previous model issues and resolutions. Section 3 of this document describes preliminary LOOP simulations for both HEU and LEU fuel at beginning of cycle conditions.

2. RELAP5 Model Description

2.1. General Considerations

2.1.1. RELAP5 version

The model described in this document was developed for RELAP5/Mod 3.3 [6]. Throughout the remainder of this document, RELAP5/Mod 3.3 will be referred to as RELAP5.

2.1.2. Solution method

The options selected for running the RELAP5 simulations summed to control option 7, which means the following options have been implemented:

- The hydrodynamics advancement setting was selected; it uses a mass error analysis to control the time step between the minimum and maximum time step (set to 1.1e-12 s and 0.1 s, respectively).
- The heat conduction/transfer time step was set to be the same as the hydrodynamic time step.
- The heat conduction/transfer and hydrodynamics were coupled implicitly (to avoid calculation failure, the explicit method was used to achieve steady-state conditions before switching to the implicit method).

2.1.3. Coolant volumes

Coolant volumes within the model were largely based on the piping system extracted from the RHF CATHARE model [2], component descriptions provided in the SAR [3] and vessel dimension provided in Ref [7]. Default parameters for coolant volumes are given here:

The volume control flags tlpvbfe for *pipe* and *snglvol* components were by default set to 0000000:

- t=0: no thermal front tracking
- l=0: no mixture level tracking
- p=0: water packing scheme used
- v=0: vertical stratification model used
- b=0: pipe interphase friction model used
- f=0: wall friction along x-axis calculated
- e=0: non-equilibrium model used

The junction control flags efvcahs for *pipe* and *sngljun* component were by default set to 0001000:

- e=0: modified PV term not used
- f=0: CCFL model not applied
- v=0: option not available
- c=1: choking model not applied
- a=0: smooth area change
- h=0: non-homogeneous model applied
- s=0: momentum flux both to and from volume

The hydraulic diameter and area for tube geometries were by default set to 0 at all junctions (internally calculated). For all other geometries only the area was set to 0 (internally set to the smallest value of the neighboring volumes). The hydraulic diameter was manually set to the smallest of the neighboring cell values.

Wall roughness for all surfaces was by default set to a small value (1.0e-6 m). This value is not expected to significantly affect RELAP5 simulation results.

Exceptions to the above default parameters are discussed in the applicable sections below.

Note that unless specified otherwise, minor loss coefficients quoted in this document were applied to both the forward and reverse flow direction.

2.1.4. Heat structures

Heat structures were included for almost all pipes in the model and for a majority of the reactor vessel and its internals. Heat structures throughout the model were discretized into 3 radial regions (4 nodes). The following default parameters were set for the heat structure components without heat generation:

- the 9 word format was selected
- convection boundary = 101 (default convection correlations)
- heat transfer hydraulic diameter = 0 (i.e. same as volume hydraulic diameter)
- the forward and reverse heated length = 100 (i.e. neglect entrance effects)
- forward and reverse loss coefficients = 0 (not required for current geometry)
- local boiling factor = 1.0 (no heat generation)

Exceptions to the above default parameters are discussed in the applicable sections below.

2.1.5. Materials

Table 1 lists the RELAP5 model materials and their temperature independent properties. Properties for the materials 1-4 were obtained from Ref. [8]. The properties for the cladding material, AlFeNi, were obtained from [6]. Materials 6, 7 and 8 were obtained from available online sources [9], [10] and [11], respectively.

Table 1 Material Properties used in RELAP5 model.

RELAP5 #	Material	Applies to:	Density	Specific Heat	Heat Capacity	Thermal Conductivity
			[kg/m^3]	[J/kg-K]	[J/m^3-K]	[W/m-K]
1	UAl_x-Al	HEU @ BOC	3580	646	2.3124e6	80
2	UAl_x-Al	HEU @ EOC	3580	646	2.3124e6	69
3	U-7Mo-Al	LEU @ BOC	9870	275	2.7143e6	66
4	U-7Mo-Al	LEU @ EOC	9870	275	2.7143e6	41
5	AlFeNi	Cladding / piping/ control rod	2702	903	2.4399e6	130
6	INOX316	Piping	7990	500	3.9950e6	16.2
7	D2O	Chimney	1100	4200	4.6200e6	0.63
8	Ni201	Control Rod	8900	440	3.9160e6	70

2.2. Model Overview

The RHF model shown in Figure 1 consists of the primary loop, CRAB loop, pressurizer, anti-syphon line, three sets of natural circulation lines and the reactor vessel. Figure 2 shows the RELAP5 model representation, including the volume numbers, for the RHF piping system. The geometry of the piping system originates from the CATHARE model supplied by the RHF team [2]; Table 2 provides a very brief summary of the systems described in detail in the following sections. The numbering convention is sequential for a given system.

Table 2 RHF piping systems

Piping System	RELAP5 Volumes	Typical Pipe Diameter (m)	Pipe Length Modeled in RELAP5 (m)	Flow Rate, Normal Operation (m3/h and kg/s)
Primary Loop	120-256	0.40	82	2407 / 735.5
CRAB Loop	452-470	0.08	6	81.5 / 24.9
Anti-Siphon Line	472-488	0.016	1.8	4 / 1.2
Pressurizer	260-264	0.06	10	16 / 4.9
Natural Circulation Lines				
Primary Loop	276-288	0.14	1.9	0 / 0
Chimney (x3)	500-504	0.08	1.2	0 / 0
CRAB Loop	464-468	0.08	1.8	0 / 0

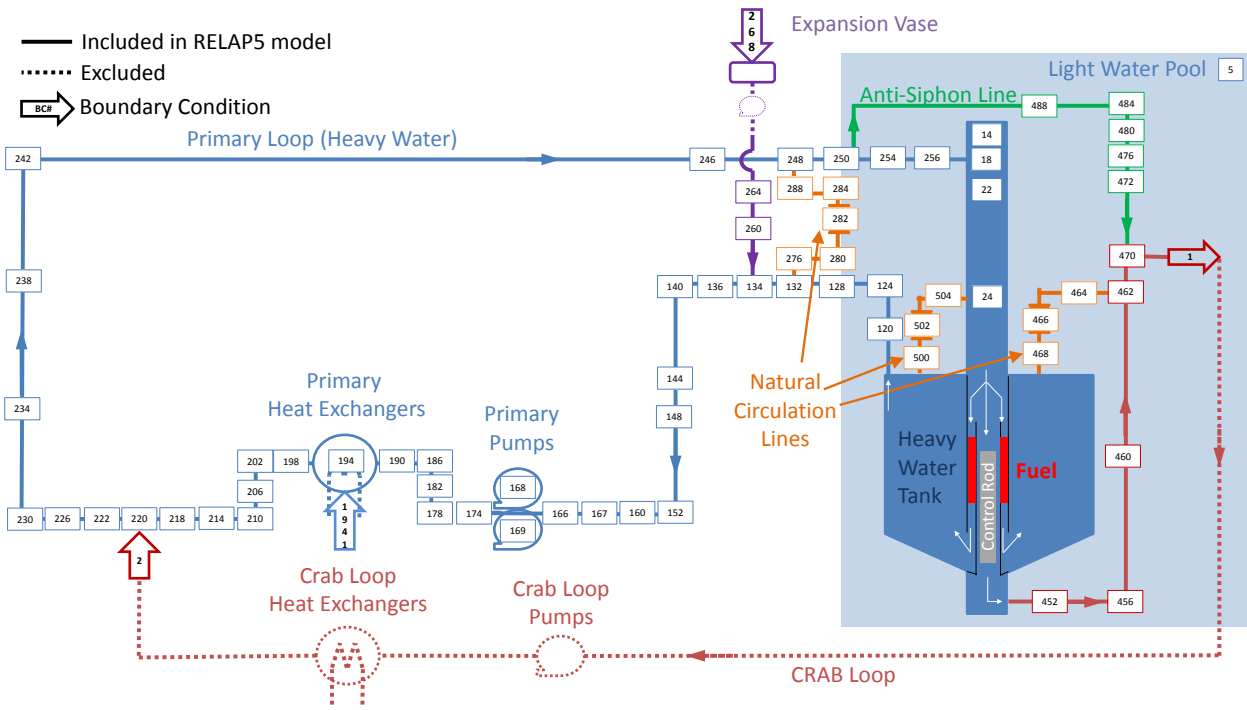

Figure 2 Conceptual drawing of RHF with RELAP5 Volumes (volumes inside heavy water tank not shown)

2.3. Primary Loop (Blue)

The primary loop, as defined here, begins with a single pipe extending out of the top of the heavy water tank. This pipe contains a 180 degree bend that directs coolant below the reactor. This configuration is meant to prevent complete draining of the tank following a pipe break. The pressurizer connects to the primary loop at the top of the 180 degree bend. Once below the reactor, the coolant is sent to the two primary pumps followed by two heat exchangers, both of which operate in parallel. The parallel piping for each of these has been consolidated into a single pipe with equivalent flow area and hydraulic diameter. Following the heat exchangers, the primary coolant mixes with the output of the CRAB loop and returns to the chimney above the reactor vessel.

2.3.1. Measurement locations

Reactor data for the primary loop was obtained from measurements made in room A13 of the RHF facility [3]. According to plant diagrams, these measurement locations are located just above the pipe elbows directly below the reactor. This is consistent with a pressure head of 0.6025 bar utilized by the RHF engineers to calculate the core exit pressure and equates to measurements being made at a plant elevation of ~205.8 m (Figure 3). More specifically, a document describing the CATHARE model [2] states the reactor inlet measurement location at 6.123 m downstream from the start of the pipe labeled BF1. This is equivalent to RELAP5 volume 234(1)[1]. The reactor outlet measurement location is described as 9.596 m downstream from the start of the pipe labeled BC2. This is equivalent to RELAP5 volume 148(3).

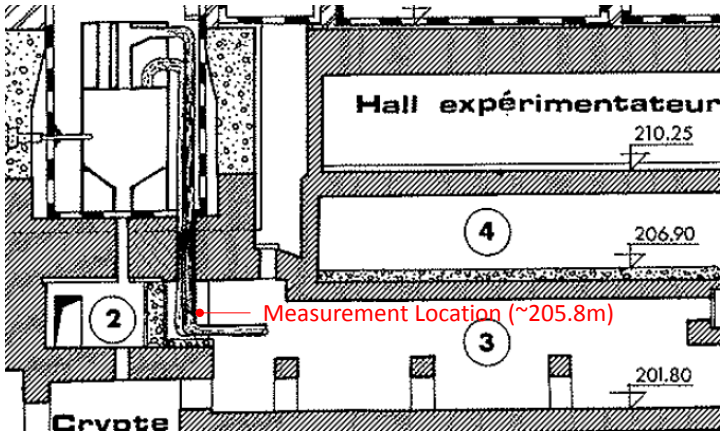

Figure 3 Pressure measurement locations in the RHF facility [3].

2.3.2. Heat structures

All of the piping was designated as AlFeNi except for the primary loop piping spanning volumes 148 through 214, which was INOX316 (stainless steel 316). Piping located within the light water pool was thermally connected to RELAP5 volume 5 (pool modeled as an infinite energy sink). Piping located outside the pool utilized a constant temperature (293K) and heat transfer coefficient (10 W/m^2-K) boundary condition to approximate the surrounding atmospheric conditions.

2.3.3. Minor loss coefficients in pipes

Standard loss coefficients for the primary loop elbows given in Table 3 where calculated based on Idel'chik [12].

[1] As a convention, the node number N of a pipe component number CCC will be referred to as CCC(N).

Table 3 Minor loss coefficients for elbows in the primary loop

Description	Idel'chik Diagram	Approximate radius (m)	Diameter (m)	Loss Coefficient	Application Point in RELAP5
Smooth elbow with $R/D > 1.5$ and $0 < \theta \leq 180$	6-2	1.252	0.394	0.218	152(3)
		1.252	0.394	0.218	230(3)
		1.066	0.400	0.212	242(2)
Sharp bends with $0.5 < R/D < 1.5$ and $0 < \theta \leq 180$	6-1	0.509	0.440	0.232	178(1)
		0.431	0.440	0.243	186(1)
		0.509	0.440	0.232	210(1)

The loss coefficient for the 180° bend downstream of the reactor vessel was determined in Ref. [12] to be 0.312. This value was equally distributed across junctions 122, 126, 138, and 142.

A minor loss coefficient was also implemented at the junction of the primary loop and the chimney. This is a complicated geometry consisting of an asymmetrically expanding pipe connected to the RHF chimney. The chimney wall contains several large, square openings that allow coolant to pass through the wall. The loss coefficient for this junction was determined by utilizing Figure 23.18 of the SAR [3]. The figure indicates a pressure loss of 0.3 bar for a velocity of 5 m/s in the chimney (area of 0.141 m). This junction is represented by volume 18(2) of the RELAP5 model (area = 0.238 m^2) and its loss coefficient was determined to be 3.09. This value was also applied to the reverse loss coefficient.

2.3.4. Primary pump

The RHF primary pump specifications provided in Table 24.6 of the SAR [3] are summarized here in Table 4. Both primary pumps have been explicitly modeled in RELAP5 and are based on the SAR specifications where possible. The flow area in RELAP5 was based on the inlet and outlet piping diameters (0.3 m). The pump length (1.44 m) was chosen to match the volume (0.102 m^3) given in the SAR specifications.

For the pump model, no two-phase operating options have been included for LOOP simulations as they are not required. The 'no-reverse' option has been selected and the reverse minor loss coefficient has been set to 9e9 to prevent any reverse flow.

Table 4 Primary pump specifications.

	SAR (1 pump)	CATHARE (2 pumps)	RELAP5 (1 pump)
Geometry			
Pipe inlet diameter	0.3 m	0.444 m	0.3 m
Pipe outlet diameter	0.3 m	0.444 m	0.3 m
Coolant volume	0.102 m^3	0.204 m^3	0.102 m^3
Length		1.32 m	1.44 m
Flow area		0.15483 m^2	0.070686 m^2
Characteristics			
Speed (100%)	2960 rpm	2970 rpm	309.97 rev/s (2960 rpm)
Flow (100%)	1090 m^3/h	2407 m^3/h	1090 m^3/h
Head (100%)	129 m	~127 m	129 m
Pump Power (torque)	600 kW	3200 N-m	1935.6 N-m
Rated Density			1100 kg/m^3
Inertia	205 kg-m^2	430 kg-m^2	205 kg-m^2
Homologous Curves		Yes	Based on CATHARE
Torque Friction -Coefficient 1 -Coefficient 2 -Coefficient 3 -Coefficient 4		 4.65 0.26 0.0 0.0	 Determined from loss of flow tests

The homologous curves were extracted from the CATHARE model and implemented in RELAP5 (Table 5). However, on closer inspection it seems that only the normal operating regime has been modeled while the others have been filled with temporary data. The homologous curves may need to be revisited if any of the accident scenarios require pump operation outside of normal conditions. The target flow rate of 735.5 kg/s was achieved by setting the pump velocity ratio to 0.948.

Table 5 Homologous curves implemented in RELAP5 model (normal operation)[2].

v/α	h/α^2	β/α^2	α/v	h/v^2	β/v^2
0	1.208	0.559	0	-0.5	-0.45
0.1	1.198	0.588	0.1	-0.42	-0.3
0.2	1.193	0.628	0.2	-0.3	-0.2
0.3	1.178	0.663	0.3	-0.01	-0.1
0.4	1.168	0.706	0.4	0.008	0.1
0.5	1.158	0.745	0.5	0.1	0.3
0.6	1.14	0.800	0.6	0.139	0.438
0.7	1.133	0.853	0.7	0.358	0.567
0.8	1.098	0.902	0.8	0.541	0.702
0.9	1.046	0.951	0.9	0.754	0.858
1	1	1	1	1	1

[2] α = rotational ratio; v = volumetric flow ratio; h = head ratio; and β = torque ratio.

In 1987 a loss-of-power experiment was performed at RHF for cold conditions and included a measurement of the pump coast-down flow rate (Figure 4). This flow rate measurement was used as the basis for specifying the RELAP5 pump coast down. RHF engineers have suggested that the flow measurement is unreliable below about 10% of the nominal flow. Due to this uncertainty, two idealized coast-down curves were proposed to bound the expected flow rate. The first coast-down curve (lower bound) assumes that the slope in measured flow rate at 10% of the nominal flow remains constant until the flow rate reaches zero. The second coast-down curve (upper bound) assumes the slope in measured flow rate at the end of the data set remains constant until the flow rate reaches zero. Approximations to these idealized coast-down curves were achieved in RELAP5 by adjusting the torque friction coefficient for the pumps. Two sets of torque friction coefficients were specified to modify the time that flow approaches zero (Table 6). The coefficients are related to the torque friction by:

$$friction\ torque = TF0 + TF1 \cdot S + TF2 \cdot S^2 + TF3 \cdot S^3$$

where 'S' is the ratio of current speed to rated speed.

Table 6 Torque friction coefficients.

	TF0	TF1	TF2	TF3
Lower Bound	10	700	3300	0
Upper Bound	-30	740	3310	0

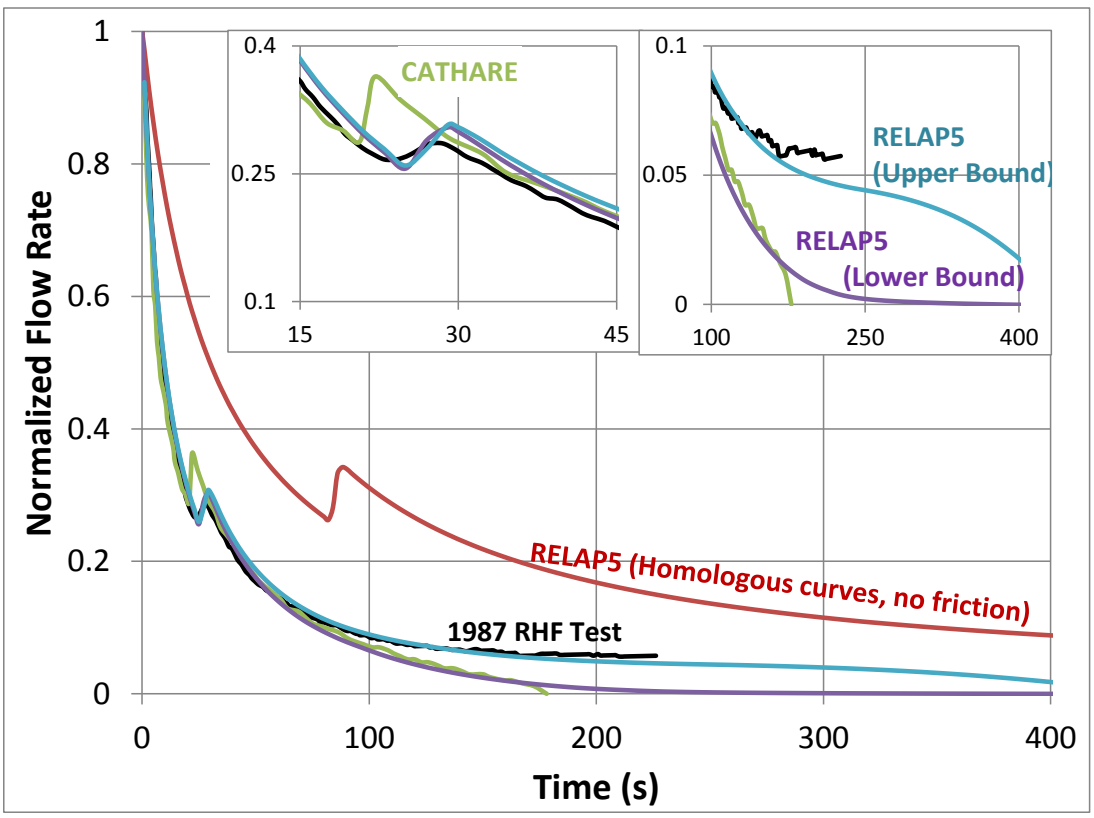

Figure 4 Measured and simulated primary pump coast down.

Figure 4 compares the RELAP5 simulated pump coast-down flow rate to the 1987 loss-of-power data using these two sets of torque friction coefficients. The simulation results show that there is about a 200 s difference in the time that the flow rate approaches zero for the upper and lower bound cases. Also shown are the results from a CATHARE model that is also based on the assumptions used in the lower bound case or the RELAP5 model. As will be discussed later, the brief increase in flow 30 s after pump trip was due to the opening of the natural circulation valves which allows part of the flow to bypass the fuel element, effectively reducing the overall resistance of the primary loop.

2.3.5. Primary heat exchangers

The heat exchanger components modeled in RELAP5 were based on a design drawing (drawing number 4C-51-P1-001) supplied by the RHF team (Figure 5) and the information provided in the Table 24.4 in the SAR [3]. This information is summarized in Table 7. There are two heat exchangers that operate with the primary coolant (D_2O) on the shell side and the DRAC river water (H_2O) on the tube side. The H_2O enters an inlet plenum which directs the water into 1040 tubes of 17 mm ID. These tubes are 6.02 m long. Water exits the tubes into a transition plenum and then returns down the remaining 1040 tubes into an outlet plenum. The D_2O enter the shell side of the heat exchanger and travels along the outside of 1040 tubes, turns around, and flows along the OD of the remaining 1040 tubes before exiting the heat exchanger. Based on a shell ID of 1.25 m, the total D_2O volume was calculated to be 3.43 m^3. This is similar to the manufacturer's specified volume of 3.4 m^3.

To simplify the RELAP5 model, the shell side of each heat exchanger has been lumped into a single component with equivalent thermal-hydraulic characteristics. The tube side of the heat exchanger was modeled with a temperature and heat transfer coefficient boundary condition. The heat transfer coefficient was specified as 4000 W/m^2-K and the temperature on the secondary side was set to control the core inlet temperature.

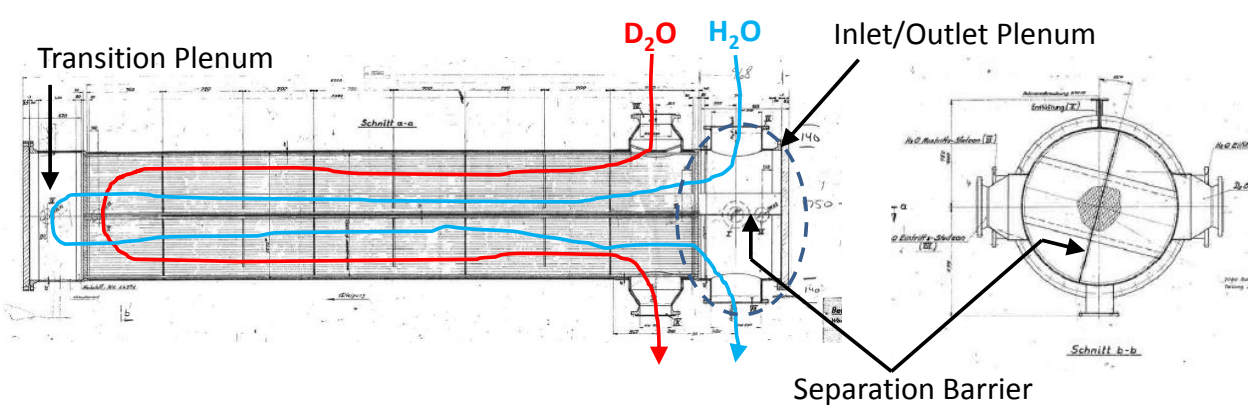

Figure 5 RHF primary heat exchanger (modified from drawing 4C-51-P1-001).

Table 7 RHF heat exchanger description

Parameter	Value	Units	Comments
Number of heat exchangers	2		Modeled as 1 equivalent heat exchanger in RELAP5
HX Drawing (drawing 4C-51-P1-001) Specifications			
Number of tubes	2080		Information from SAR [3]
Tube outer diameter	0.02	m	
Tube wall thickness	0.0015	m	
HX tube length	6.02	m	
Shell inner diameter	1.25	m	
Calculated Parameters			
Tube wetted perimeter	65.35	m	These numbers represent half of the heat exchanger
Shell wetted perimeter	3.21	m	
Total wetted perimeter	68.56	m	
Tube area	0.33	m^2	
Shell area	0.61	m^2	
Total area	0.29	m^2	
Tube volume	1.97	m^3	
Shell volume	3.69	m^3	
Total volume	1.73	m^3	
Total volume (x2)	3.45	m^3	Total volume within heat exchanger
Actual	3.40	m^3	Information from SAR [3]
RELAP5 VOLUME (194)			
Divisions	20		
Total length	12.04	m	Equivalent heat exchanger utilizes length from 1 heat exchanger
Unit length	0.602	m	
Area	0.57	m^2	Based on 2 heat exchangers
Hydraulic diameter	0.017	m	4 x flow area / wetted perimeter of cross section
RELAP5 HEAT STRUCTURE (1941)			
Divisions	20		
Left boundary	0.0085	m	Inner radius of a tube
Right boundary	0.01	m	Outer radius of a tube
Cylinder height / division	1252.16	m	Accounts for all tubes in both heat exchangers

The inlet and outlet to the heat exchangers was modeled with junctions 193 and 195, respectively. The abrupt area change model was implemented at these junctions. Pipes 190 and 198 were considered to be a consolidation of parallel pipes, thus the hydraulic diameter was specified as 0.3 m with a flow area equivalent to two pipes. The heat exchanger specified pressure drop was 1.16 bar at a nominal flow rate of 1090 m^3/h (Table 24.4 of the SAR [3]). In RELAP5, this pressure drop was evaluated between volumes 190 and 198. A total loss factor of 158.8 was required to achieve the target pressure drop. This loss coefficient is quite high but can be justified by the fact that the heat exchanger design includes internal baffles that create a torturous coolant path. This loss factor was distributed equally between the 19 junctions within pipe 194 (heat exchanger).

2.4. CRAB Loop (Red)

The CRAB loop, as defined here, begins at the pipe connection near the bottom of the heavy water tank. Similar to the primary loop, the piping ascends above the heavy water tank prior to a 180 degree bend that redirects the coolant downward below the reactor vessel. The CRAB loop has only been partially modeled in RELAP5 since this was the approach taken in the CATHARE model and additional information would be required to incorporate it[3]. The section of the CRAB loop downstream from the anti-syphon line has been removed and replaced with an outlet mass flow boundary condition (BC 1 in RELAP5 model). It represents the combined flow of the anti-syphon line and control rod. This coolant was reintroduced into the primary loop at volume 220 with an inlet mass flow and temperature boundary condition. The section of CRAB loop not included in the model should not significantly contribute to accident conditions[4] since the pump coast down data shows that the flow rate approaches zero in approximately 6 seconds, much faster than the primary pumps (approximately 200-400 seconds).

2.4.1. Heat structures

All of the CRAB loop piping was designated as AG3NET with a 4.5e-3 m wall thickness. The only exception to this was RELAP5 volume 470 (junction of CRAB loop, anti-syphon and outflow boundary condition). Here, no heat structure was modeled in CATHARE since no information was available. The CRAB loop piping is located within the light water pool and was thermally connected to RELAP5 volume 5 (pool modeled as an infinite energy sink).

2.4.2. Minor loss coefficients

A single minor loss coefficient was included in the CRAB loop and was applied to the elbow designated by volume 456 (Table 8).

Table 8 Minor loss coefficient for CRAB loop elbow.

Description	Idel'chik Diagram	Approximate radius (m)	diameter (m)	Loss Coefficient	Application point in RELAP5
Smooth elbow with R/D > 1.5 and 0 < t ≤ 180	6-2	0.24	0.08	0.216	Split between junctions 454 and 458

2.4.3. Loss of flow

The CRAB loop flow rate decreases rapidly following a loss of flow (~6 s). Discussion with RHF engineers led to the following normalized coast down flow in the CRAB loop for use in RELAP5 (Table 9). The target flow rate was based on the reference steady-state mass flow rate (defined in Table 20).

[3] The CRAB piping dimensions would be required. Table 24.5 and 24.7 of the SAR contain enough information to model the 3 heat exchangers and the pumps (although it doesn't provide the pumps inertia value or homologous curves).

[4] This may need to be re-evaluated depending on the models application.

Table 9 Target CRAB flow rate as determined from loss of flow tests.

Time after trip (s)	Normalized flow rate	Target flow rate (kg/s)
0	1	24.9
0.5	0.85	21.165
1	0.6	14.94
1.2	0.4	9.96
1.5	0.3	7.47
2.2	0.2	4.98
3.4	0.1	2.49
3.9	0.08	1.992
4.4	0.04	0.996
6	0.02	0.498
7.6	0.002	0.0498
8	0	0

2.5. Anti-Syphon Line (Green)

The anti-syphon line connects the upper elevation of the CRAB loop to the primary inlet piping and is intended to prevent a break in the CRAB loop from syphoning coolant from the core.

2.5.1. Heat structures

All of the anti-syphon piping was designated as AG3NET with a 2.0e-3 m wall thickness. This piping is located within the light water pool and was thermally connected to RELAP5 volume 5 (pool with infinite energy sink).

2.5.2. Minor loss coefficients

The anti-syphon line contains two elbows. The first is represented in RELAP5 by volume 480 and was treated as a smooth elbow with radius to hydraulic diameter ratio of 22. The loss coefficient was determined to be 0.74 from Table 6-2 of Ref. [12].

The second elbow was considered to be a smooth, sharp angled elbow and its loss coefficient was calculated to be 1.2 based on Table 6-1 of Ref. [12] (radius to hydraulic diameter ratio of ~0.5). The loss coefficient was applied to junction 486.

The anti-syphon line inlet connection is to RELAP5 volume 250. Based on the description in the CATHARE model this is a horizontal tee. The cross flow junction model was used by connecting to face 6 of branch 250. As described in Appendix A, the forward and reverse loss coefficients were 3.005 and 1.0, respectively. These were applied to junction 489.

No loss coefficient was specified for the connection of the anti-syphon line and the CRAB loop. This will need to be revisited if the CRAB loop piping is implemented.

2.6. Pressurizer (Purple)

The RHF pressurizer connects to the top of the 180 degree bend in the primary loop piping downstream from the reactor core. The reactor pressure is controlled by two pressurization pumps operated in parallel (~18 m^3/hr). These pumps are identical to those used in the CRAB loop. The pumps obtain water from an expansion vase containing heavy water maintained at a facility elevation of

223.509 ± 0.191 m (SAR 241.1.3.8 [3]). Under normal operation, the expansion vase water is replenished by small diameter piping connected to the top of the vessel chimney and reflector tank. A low pressure helium cover gas system maintains the expansion vase pressure at slightly above atmospheric pressure (1.06 bar). In the RELAP5 model, the pressurizer model includes the total heavy water volume of the pressurizer connected to a pressure/temperature boundary condition (Figure 6). The pumps have not been included in the model. The connecting pressurizer pipe dimensions were modeled similar to the CATHARE model but its height was adjusted such that the top of the heavy water volume was 223.509 m, relative to the core mid-plane value of 211.8 m. An isolation valve has been included to prevent a continuous water supply for loss-of-coolant accident (LOCA) simulations.

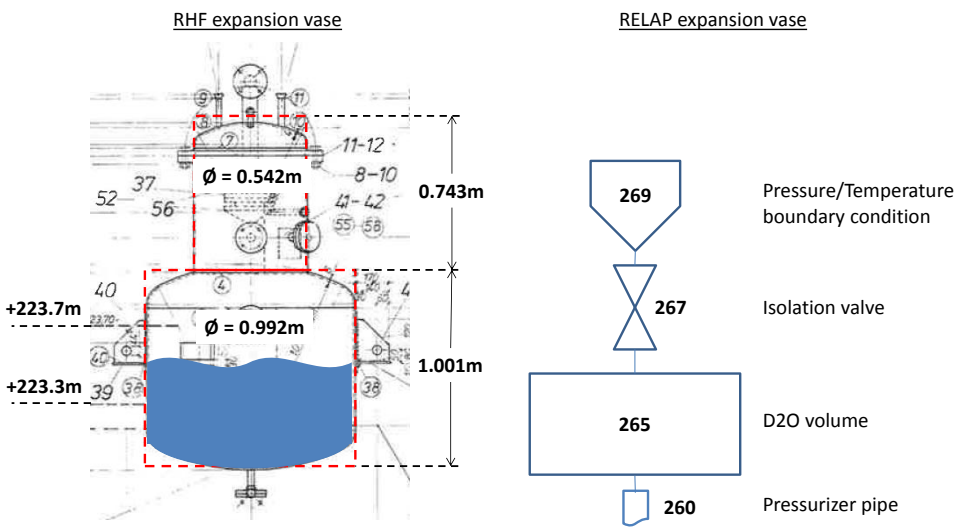

Figure 6 RHF expansion vase.

2.6.1. Heat structures

No heat structures were included in the pressurizer model.

2.6.2. Minor loss coefficients

The pressurizer connection to the primary loop utilized the cross flow junction model by connecting to face 6 of branch 134. As described in Appendix A, the forward and reverse loss coefficients were 6.083 and 8.12, respectively.

2.6.3. Loss of flow

Following discussions with the RHF engineers, it was decided that the time dependent pressure for accident simulations would be based on the 1987 loss of flow data [5]. The target pressures shown in Table 10 have been reduced by 0.34 bar relative to the 1987 data so that the reference normal operation outlet pressure was 4.0 bars. Table 10 also shows the boundary condition pressure required to achieve the target pressure at RELAP5 volume 148(3). In addition, the boundary condition pressure 14 s and beyond was reduced an additional 0.25 bar to better match the target pressure at RELAP5 volume 148(3). Figure 7 shows the RELAP5 simulation results compared to the target pressure at the primary loop outlet measurement location. The RELAP5 simulated pressure did not evolve smoothly as oscillations occurred up to 50 s beyond the trip. These oscillations are likely due to the approximation of

the pressurizer as an imposed boundary condition but should not have a significant effect on simulation results for a LOOP accident.

Table 10 Target coast down pressure and the required pressure at RELAP5 boundary condition.

Time after trip (sec)	Target Pressure (bars)	Boundary condition (bars)	Time after trip (sec)	Target Pressure (bars)	Boundary condition (bars)
0.00	4	2.21	4.08	3.49	1.8
0.16	4.1	2.41	4.24	3.46	1.77
0.39	4.25	2.56	4.94	3.32	1.63
0.71	4.3	2.61	5.24	3.26	1.57
0.85	4.32	2.63	6.10	3.14	1.45
1.18	4.26	2.57	7.31	2.97	1.28
1.41	4.22	2.53	7.72	2.91	1.22
1.65	4.17	2.48	8.93	2.75	1.06
1.77	4.15	2.46	9.11	2.72	1.03
1.89	4.11	2.42	10.54	2.53	0.84
2.24	3.98	2.29	12.12	2.43	0.74
2.36	3.95	2.26	12.85	2.38	0.69
2.83	3.83	2.14	13.27	2.36	0.67
2.93	3.81	2.12	14.00	2.33	0.39
3.07	3.77	2.08	15.00	2.3	0.36
3.54	3.64	1.95	15.00+	2.3	0.36

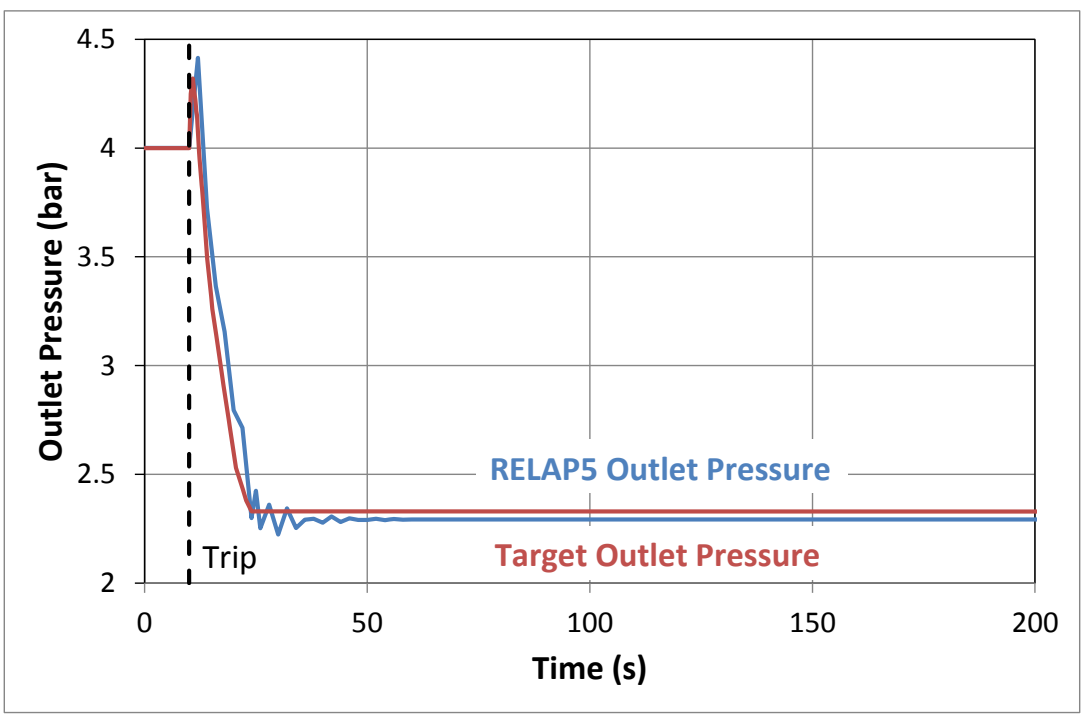

Figure 7 Comparison of target and RELAP5 simulated outlet pressure.

2.7. Natural circulation (Orange)

Three natural circulation pipes were modeled in RELAP5 (Figure 1 and Figure 2). The first natural circulation pipe connects the chimney to the reflector region of the heavy water tank. This model is actually a consolidation of three parallel pipes and valves. The second natural circulation pipe is identical to one of the three previous pipes but connects the reflector region of the heavy water tank to the CRAB loop. The third natural circulation pipe connects the primary inlet and outlet pipes.

2.7.1. Heat structures

All of the natural circulation pipes were designated as AG3NET. They are also all located within the light water pool and were thermally connected to RELAP5 volume 5 (pool with infinite energy sink). The piping connected to the chimney, CRAB loop and inlet piping each had a thickness of 0.01 m, 0.0045 m and 0.01 m, respectively.

2.7.2. Valves

Each of the natural circulation pipes contains a check valve (282, 466, 502) actuated by a pressure differential between its downstream pressure and the CRAB outlet pressure (Figure 8).

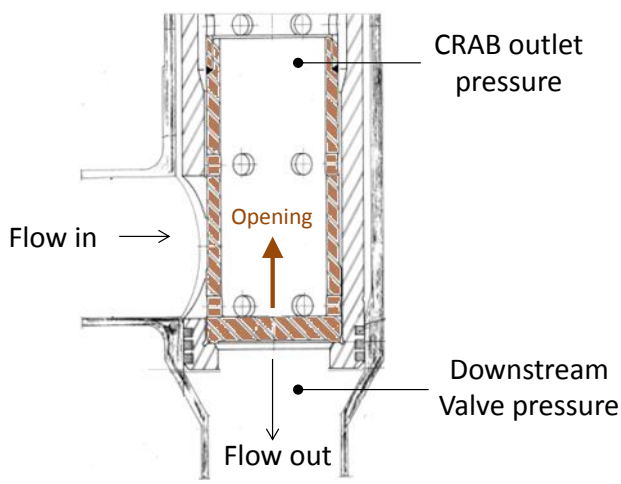

Figure 8 Diagram of a check valve in a natural circulation line

The SAR (Section 233.11.2) [3] states that the natural circulation valves open with a ~1 bar pressure differential. Because of the plurality in the wording of the SAR (valves), it was assumed that this applies to all of the natural circulation valves. A control system for each valve was implemented to compare the CRAB outlet pressure at RELAP5 volume 220 and the downstream valve pressure (Figure 9). Table 11 shows the relative elevation and pressure correction applied to the control system to capture the 1 bar differential at the valves. It was found that reducing this pressure differential limit in RELAP5 by 0.15 bar resulted in valve opening times consistent with that measured in the 1987 loss of flow tests[5]. The opening rate for the valves were based on the loss of flow tests and are representative of the time difference between the first indication of valve movement and reaching fully open.

[5] This 0.15 bar adjustment required to match experimental data is likely related to the bias in pressure head correction. The RELAP5 reference pressure is at volume 220 but the actual location of the pressure tap was only known to be downstream of the CRAB loop pumps.

Table 11 RELAP5 control system values for the natural circulation valves.

RELAP5 VALVE (#)	Relative elevation (m)	Pressure head correction (bar)	RELAP5 opening pressure differential (bar)	Calibrated pressure differential (bar)	Opening rate [s^{-1}]
282	11.12	1.200	2.200	2.050	0.176
502	9.60	1.036	2.036	1.886	0.320
466	10.39	1.121	2.121	1.971	0.248

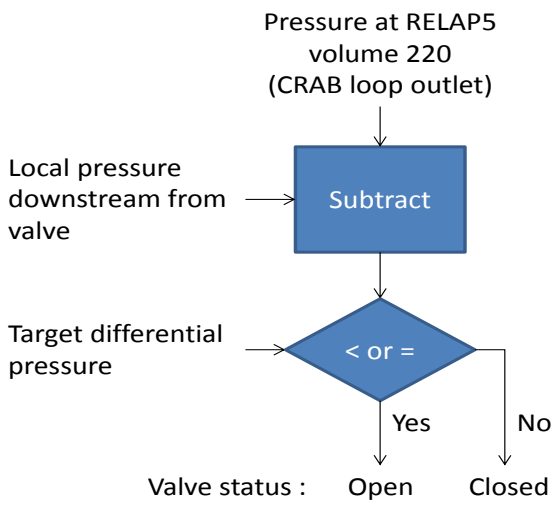

Figure 9 Control logic for natural circulation valves.

Table 12 shows the flow area as a function of valve position. The SAR states that the flow passage area is equivalent to a 70 mm diameter for valves 502 and 466 and 100 mm diameter for valve 282. The flow areas were determined by calculating the fraction of circular cross sectional area open to coolant flow due to the relative position of the valve.

Table 12 normalized flow area as a function normalized valve position.

Normalized position	Flow Area [m^2]		Normalized flow area
	502, 466	282	
0	0.000000	0.000000	0.0
0.1	0.000200	0.000409	0.052
0.2	0.000548	0.001118	0.142
0.3	0.000971	0.001982	0.252
0.4	0.001438	0.002934	0.374
0.5	0.001924	0.003927	0.5
0.6	0.002411	0.004920	0.626
0.7	0.002877	0.005872	0.748
0.8	0.003301	0.006736	0.858
0.9	0.003648	0.007445	0.948
1	0.003848	0.007854	1.0

2.7.3. Minor loss coefficients

The natural convection piping connecting the chimney to the heavy water tank (Figure 10) contained three loss coefficients. A loss coefficient of 1.2 was added to valve 502 and was based on a sharp angle elbow (r/D=0) correlation provided in Idel'chik diagram 6-7 [12]. The RELAP5 abrupt area model was applied to this valve as well as at the pipe connection at the heavy water tank. A tee was modeled at the connection to the chimney. The cross flow junction model was used by connecting to face 6 of pipe 24. As described in Appendix A, the forward and reverse loss coefficients were 22.94 and 19.923, respectively. These were applied to junction 489.

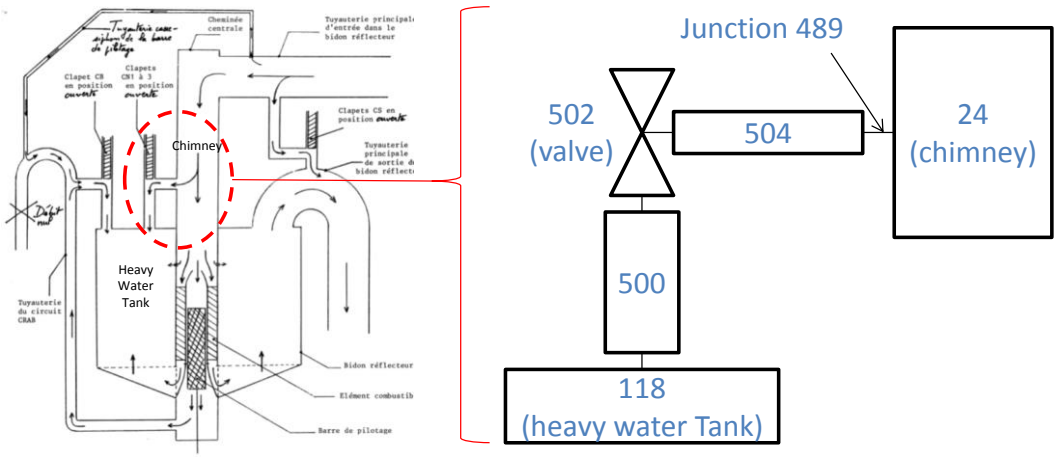

Figure 10 RELAP5 description of the natural circulation lines connecting the chimney to the heavy water tank.

The natural convection line connecting the CRAB loop to the heave water tank (Figure 11) also contained three loss coefficients. The valve and discharge into the heavy water tank were treated that same as above. Connection to the CRAB loop was modeled as a symmetrical tee with cross junction connection to face 6 of branch 462. The forward and reverse loss coefficients were 1.84 (Appendix A). Similar to Valve 502, the forward and reverse loss coefficients of valve 466 were specified as 1.2.

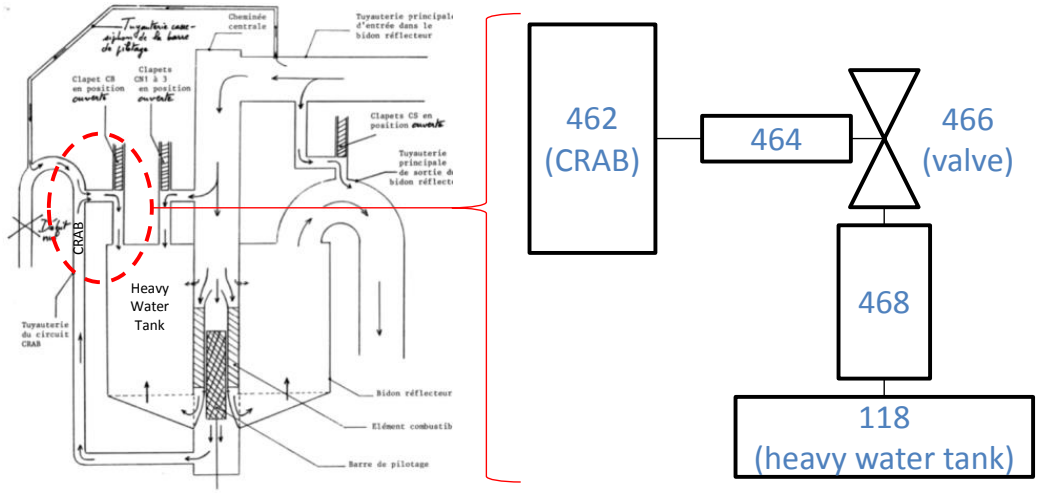

Figure 11 RELAP5 description of the natural circulation line connecting the CRAB loop to the heavy water tank.

The bypass line connecting the primary inlet piping to the primary outlet piping (Figure 12) contained five loss coefficients. The loss coefficient at the diverging wye of the inlet pipe was treated as a tee since Idel'chik does not provide a loss coefficient for the wye flow distribution following the loss of flow transient[6]. A cross flow junction to face 6 of branch 248 was used to represent this junction. As described in Appendix A, the forward and reverse loss coefficients were 8.461 and 5.847, respectively. A loss coefficient of 1.2 was applied to two 90 degree sharp elbows (junction 286 and 278) and valve 282. The tee connection to the primary outlet piping was modeled with a cross flow junction to face 6 of branch 132. As described in Appendix A, the forward and reverse loss coefficients were 3.762 and 5.315, respectively.

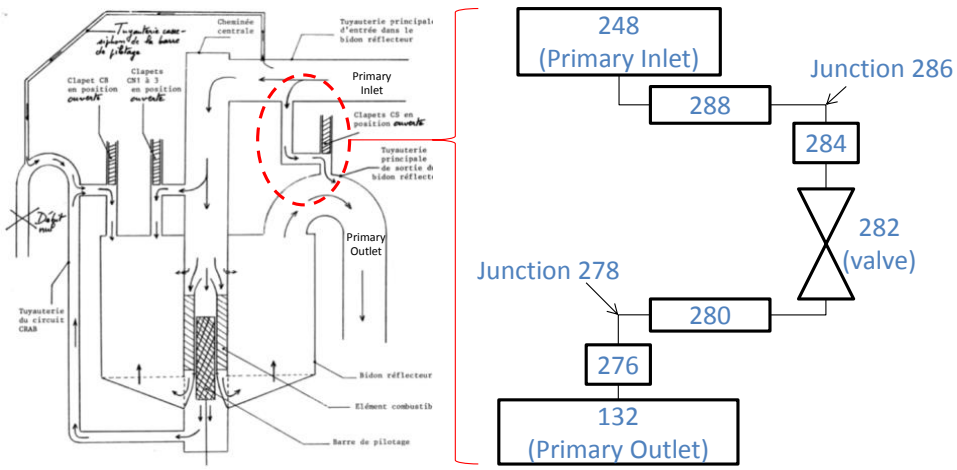

Figure 12 RELAP5 description of the natural circulation line connecting the in the primary inlet and outlet piping.

2.8. RHF Reactor Vessel

Figure 13 shows a conceptual drawing of the reactor vessel, or heavy water tank, and its internal components. The primary loop piping connects to a central chimney extending from the top of the heavy water tank. Coolant flows down the chimney and enters the heavy water tank at RELAP5 volume 28. Volumes 28 and 30 are a continuation of the chimney volumes penetrating the vessel. Coolant splits between the primary loop (through the fuel element) and CRAB loop (through the control rod). A small amount of coolant bypasses the fuel element and enters the reflector region directly.

The RELAP5 model discretization of the fluid within the reactor vessel consists of the fuel element, control rod and reflector regions. Figure 13 also illustrates the heat structures of the reactor vessel and their links to the coolant volumes. Lines connecting coolant volumes indicate a thermal connection through a structure. Lines arcing from a structure and pointing to the coolant indicate heat generation within the coolant volume and the structure which is used to define its magnitude. (In RELAP5, the magnitude of heat generation within the coolant is defined by an adjacent heat structure). A table describing the detailed power generation within the RHF core and vessel were obtained from MCNP calculations for both HEU and LEU fuel at BOC conditions. This heat generation (indicated by a star in

[6] This approximation is not expected to have a significant impact on simulation results.

Figure 13) was also modeled within the control rod tubes, fuel plates, and vessel walls as detailed in the following sections.

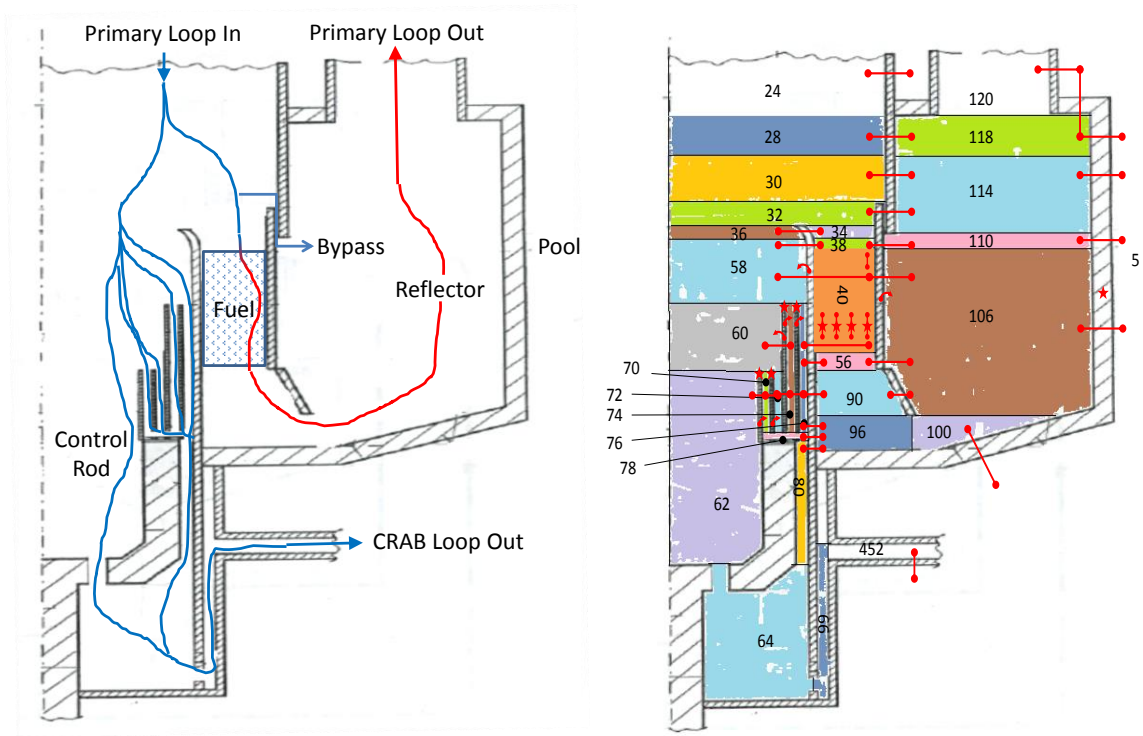

Figure 13. Coolant volume discretization scheme and heat structure linkages in RELAP5 model.

2.8.1. Control rod

The entry into the control rod region (volume 36) corresponds to the inner section of the "conical head" with varying diameter (Figure 14). The flow area of 0.0354 m^2 for volume 36 was based on the volume of a conical frustum of equivalent upper and lower diameters. Volume 58 represents the coolant above the control rod and its length depends on the control rod tip axial position. The control rod consists of four vertical, annular cylinders at the end of a traversing system that moves the control rod up and down depending on neutronic requirements. In the reference RELAP5 model the top of the control rod is placed at the core mid-plane[7]. Table 13 describes the geometry of the various coolant volumes within the control rod. The coolant paths within the control rod converge into volume 64, representing the region below the control rod. The length of this region is related to the length of volume 58 above the control rod since the overall length of the control rod region remains fixed for all control rod position. The junction between volumes 62 and 64 was modeled based on a drawing (drawing number 3-54-P1-1003-8) that indicates there are three coolant holes with a diameter of 0.011 m. The lower end of volume 64 is connected to volume 66 which connects to the CRAB loop piping. It should be noted that the control rod has a complex design and its representation in RELAP5 is mostly based on the CATHARE model, which in itself is rather complex. Because of this, volumes and junctions connected to volume 64 are quite simplified relative to design drawings.

[7] The control rod position has been fixed for the current stage of RELAP5 model development and thermal-hydraulic analyses.

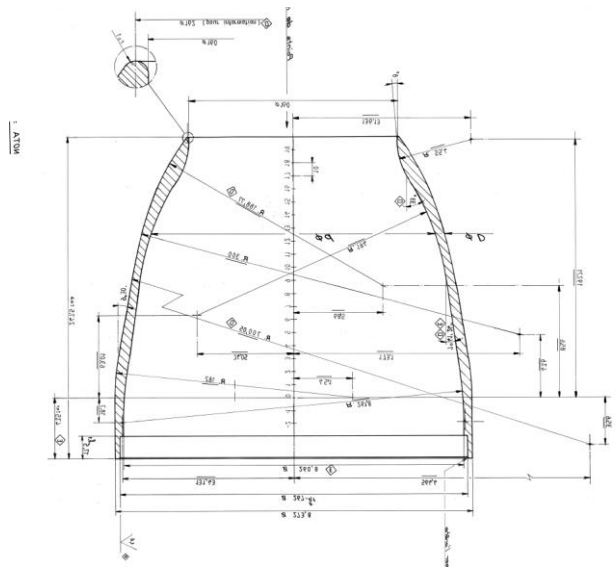

Figure 14 Diagram of the conical head separating the flow between the control rod and fuel element regions.

Table 13 Geometry of the control rod coolant volumes.

RELAP5 Volume	Geometry	Inner Radius [m]	Outer Radius [m]	Flow Area [m^2]	Length (m)
60	Cylinder	-	0.1074	3.6238e-2	0.598
62	Cylinder	-	0.0901	2.5503e-2	1.377
70	Annulus	0.0942	0.0978	2.1715e-3	0.357
72	Annulus	0.1038	0.1074	2.3886e-3	0.357
74	Annulus	0.1114	0.1184	5.5036e-3	0.955
76	Annulus	0.1244	0.1304	4.8029e-3	0.955
78	Annulus	0.0942	0.1304	6.6607e-3	0.920
80	Annulus	0.1220	0.1304	1.4700e-2	0.101

2.8.1.1. Minor loss coefficients

Section 273.5 of SAR provides data that allows for the calibration of the flow distribution within the control rod. A summary of this data is given in Table 14 for a total flow 50 m^3/h; where the pressure drop was stated as 0.12 bar (assumed to be between RELAP5 volumes 58 and 64). Loss factors were applied at the indicated RELAP5 junctions (Table 14) to reproduce the target conditions. The abrupt area change model was applied to the junction of volumes 62 and 64.

Table 14 Control rod flow distribution summary (From Table 27.8 of the SAR)

Channel [RELAP5 junction]	Inner Diameter (mm)	Outer Diameter (mm)	SAR Table 27.8 flow rate (kg/s)	RELAP5 flow rate without loss factor (kg/s)	RELAP5 flow rate with loss factor (kg/s)	Required loss factor
Total			15.28	15.28	15.28	
Between fuel element and tall Ni tube [58(4)]	124.4	130.4	5.98	4.42	5.98	20.13
Between tall Ni and tall Al tube [58(3)]	111.4	118.4	5.10	5.19	5.10	32.12
Between tall Al and short Ni tube [60(3)]	103.8	107.4	1.72	2.71	1.72	65.14
Between short Ni and short Al tube [60(2)]	94.2	97.8	1.35	2.46	1.34	87.94
Center of control rod [60(1)]	0	90.1	1.12	0.51	1.13	0
Pressure drop			12 kPa	6 kPa	18 kPa	

It was not possible to achieve the 0.12 bar pressure drop and achieve the target flow rates. This indicates that the control rod description in the RELAP5 model, obtained from the CATHARE model, is not quite accurate. Of note is that Table 27.8 of the SAR suggests that the coolant flowing through the short control rod channels exits back into the center of the control rod as opposed to merging with the coolant from the tall control rod tubes which exit into an outer annulus. Implementing this change into the RELAP5 model would reduce the overall pressure drop; however, more detailed control rod dimensions would be required before this could be implemented. The flow rate distribution and pressure drop stated in Table 14 was considered sufficient at this time.

In addition to these losses, the abrupt area change model was applied to junction 450 (connects the bottom of the control rod volumes to the CRAB loop outlet piping).

2.8.1.2. Heat Structures

Heat structures within the control rod were limited to, as indicated in Figure 13, the tube separating the control rod coolant from the fuel element and the four control rod tubes. Heat generation was applied to the control rod tubes (heat structures 700, 720, 740 and 760), the coolant volume between them (volumes 70, 72, 74 and 76) and the coolant above and within the control rod (volumes 58 and 60). The heat generation within these coolant volumes was assumed to be uniformly distributed. In the current model no thermal connections where made in the vessel below the control rod tubes.

2.8.2. Fuel element

The fuel element consists of 280 involute plates; an example of the fuel plate is shown in Figure 15. The plate thickness is 1.27 mm with a fuel meat thickness of 0.51 mm and the coolant gap between the plates is 1.8 mm. The fuel plates are welded to concentric tubes radially bounding the coolant between 0.1369 m and 0.1988 m. These concentric tubes separate the coolant within the fuel element from the control rod and reflector regions. In the RELAP5 model, the fuel plates and coolant channels are consolidated into an equivalent single coolant channel and fuel plate. The fuel plate was discretized as shown in Figure 15. Two 'hot stripes' were defined at the outer edge of the fuel plate (heat structures 410 and 420) and another at the inner edge (heat structure 430). Note that the 3.0 mm dimension in the figure is the arc length of the involute structure. The remainder of the heated fuel plate was lumped into heat structure 400. The non-heated portion of the fuel plate was designated as heat structure 401. This discretization was based on the radial variation in the power profile. Briefly, heat structure 410 is considered to contain the peak cladding temperature for BOC conditions. Heat structure 420 and 430 are place holders for cases in which the peak clad temperature is suspected to occur inside of heat structure 410 or at the inner edge of the fuel (e.g. EOC conditions).

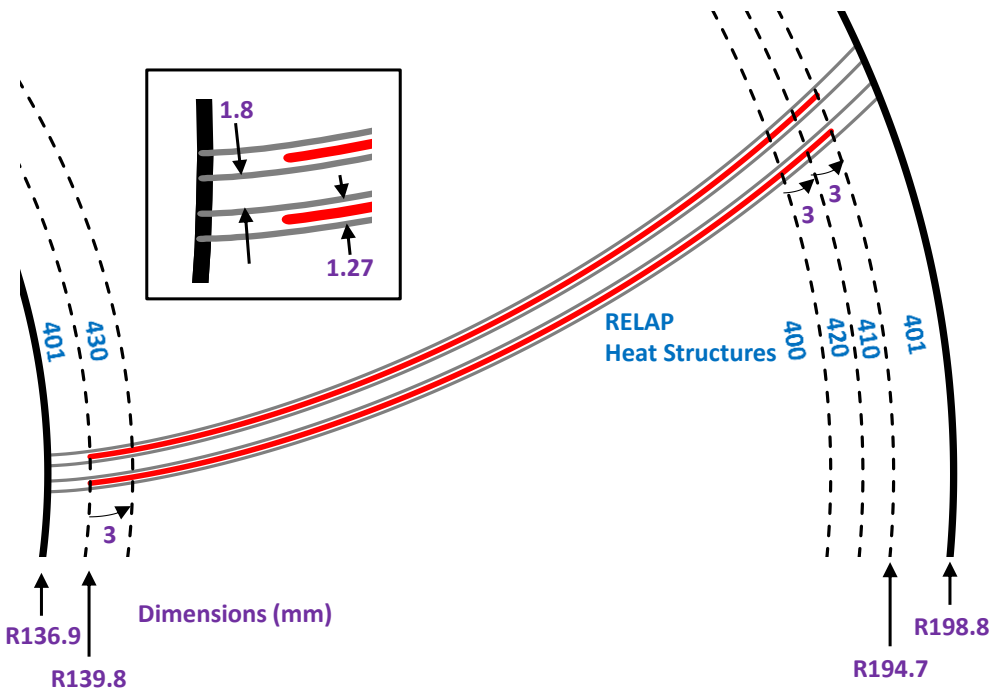

Figure 15 Discretization of the RELAP5 coolant volumes within the fuel element

Table 15 provides the critical parameters for each of the fuel plates. The coolant flow area and heat structure surface areas were determined by calculating the involute length bounded by the coolant with a gap size of 1.8 mm and channel height of 903 mm. The involute equations in Cartesian coordinates are:

$$x = a(\cos t + t \sin t); \text{ X-coordinate}$$

$$y = a(\sin t - t \cos t); \text{ Y-coordinate}$$

$$r = \sqrt{x^2 + y^2}; \text{ Radius}$$

$$l = \frac{1}{2} a t^2; \text{ Arc length}$$

where 'a' was defined as 0.1368 m.

Table 15 Fuel element geometry in RELAP5 model

RELAP5 structure	Inner/Outer Radius [mm]	Plate Arc Length [mm]	Total Flow Area [m^2]	Total Volume [m^3]	Hydraulic Diameter [m]	Total Surface Area [m^2]
401	136.9 / 139.8	2.9	1.462e-3	1.320e-3	0.003517	4.450
	194.7/ 198.8	5.9	2.974e-3	2.685e-3		
400	142.7 / 190.4	58.1	29.282e-3	26.442e-3		29.38
410	192.6/ 194.7	3.0	1.512e-3	1.365e-3		1.517
420	190.4/ 192.6	3.0	1.512e-3	1.365e-3		1.517
430	139.8 / 142.7	3.0	1.512e-3	1.365e-3		1.517
Total	136.9/194.7	75.9	0.03825	0.03454		38.381

The hydraulic diameter for coolant volume of the fuel element (40) and its internal junctions were specified as 3.517e-3 m.

RELAP5 also allows the modification of the channels shape factor; a parameter that allows the user to adjust the laminar friction factor due to the non-circular shape of the channel:

$$fRe = 24 \cdot (1 - 1.3553x + 1.9467x^2 - 1.7012x^3 + 0.9564x^4 - 0.2537x^5)$$

where 'x' is the channel width to length ratio. For a gap width of 0.0018 and an arc length of 0.0759 m, the shape factor input into the RELAP5 model was 0.688 (shape factor = 16/f-Re).

For the reference simulations, the axial discretization of the coolant volume was 24 equal spaced volumes within the heated region (0.8 m long) of the fuel element and an additional volume at the top and bottom of the unheated length (0.052 m and 0.051 m long, respectively for HEU). For the LEU simulations, the heated length was increased to 0.88 m. The number of axial volumes in the heated and unheated region remained the same but their lengths were adjusted to maintain the overall fuel element length (0.903 m).

There was no radial discretization of the coolant volume within the fuel element for the reference model; it was modeled as a single channel. A discussion supporting this approach is given in Appendix B and the results presented in Section 3. It is worth noting that the CATHARE model included a radial discretization to obtain three separate coolant channels within the fuel element.

2.8.2.1. Minor loss coefficients

The only loss coefficients in the fuel element region implemented in the RELAP5 model are from the application of the abrupt area change model to the junctions at the inlet and outlet of the fuel element.

2.8.2.2. Heat structures

The heat structures defining the fuel element were assumed to be rectangular plates with a thickness of 1.8 mm and length equal to the involute length. A heat structure was created for each of the 'hot stripes' as well as for the remaining heated and unheated section of the fuel element. In the thickness direction, the fuel element structures contained 10 nodes with 3 radial regions in each of the sections: left cladding, fuel (or center clad) and right cladding. The 12 word RELAP5 format was used to include specifying a natural convection length equal to the height of the fuel; a value used in the natural convection heat transfer correlation (Churchill and Chu, [6]) at the plate surface. The axial discretization of the heat structures was the same as the coolant. A detailed table of power density as function of radius and axial position was produced from MCNP calculations and the information was consolidated by summing the power distribution within each of the heat structure axial nodes (discussed further in Section 2.8.4).

2.8.3. Reflector

The reflector region consists of volumes 100-118 and each of these was discretized axially to match the fuel element and entry region. The reactor contains a number of structures in the reflector region for experimental purposes but these have been neglected in this model. The current RELAP5 model, as well as the CATHARE model, have a heavy water volume of 11.2 m^3, whereas a detailed hand calculation (Table 16) accounting for these structures results in a volume of ~10.3 m^3. No further changes have been made to the model at this time. It is not clear that this discrepancy in heavy water volume will have a significant effect on the simulation results, but further investigation may be necessary.

Table 16 ANL best estimate of coolant volume within heavy water tank.

Component	ANL best estimate volume (m^3)
Heavy water tank (empty)	11.205
Central chimney (within tank)	0.148
Fuel element	0.137
Grids	0.172
Beam tubes:	
H1	0.022
H2	0.029
H3	0.026
H4	0.018
H5	0.045
H6-H7	0.021
H8	0.024
H9	0.033
H10	0.038
H11	0.034
H12	0.015
H13	0.030
V4	0.003
V7	0.003
Source:	
Hot	0.080
Cold	0.035
Total	10.293

2.8.3.1. Minor loss coefficients

Entry into the reflector region is complicated by the flow turnaround and grid plates. This junction (96) was modeled with a flow area and hydraulic diameter characteristic of the grid plate (drawing Re 3C 53 GS P13 015):

- 24 + 4 x 48 holes of 1.4 cm diameter = 332.5 cm^2
- 48 gap 15.65cm long, 0.7 cm width and 2 x 48 half disk of radius 0.35cm = 544.3 cm^2
- 48 gap 15.65 cm long, 0.77 cm width and 2 x 48 half disk of radius 0.385cm = 600.8 cm^2

Total flow area through the grid was specified as 0.14776 m^2. Using the flow area and wetted perimeter, the hydraulic diameter was calculated to be 0.01338 m. The abrupt area change model was applied to this junction.

The core bypass, or leakage, is stated to be 42 m^3/h; with 85 m^3/h flowing through the control rod and 2365 m^3/h through the fuel. This leakage is modeled with a junction connecting the outlet of branch 34 with the outlet of branch 110. To achieve the target flow rate for a hydraulic diameter and flow area of 0.053 m and 2.21×10^{-3} m^2, respectively, the required loss coefficient at junction 1 of volume 34 was calculated to be 58.85. This value was applied to both the forward and reverse loss coefficient. The hydraulic diameter and flow area of the core bypass were obtained from CATHARE and no other reference was found to confirm the basis for these values.

An abrupt area change model was also applied to the primary outlet piping connection at the top of the reflector region (tank).

2.8.3.2. Heat structures

Heat structures associated with the reflector volume includes the portion of chimney pipe that penetrates into the top of the heavy water vessel, the outer cylinder of the fuel element, and the grid plate (structures 280, 402 and 900, respectively) as well as the heavy water tank bottom, side and top (structures 1001, 1061 and 1181, respectively). The dimensions used in determining these heat structures (and coolant volumes) are shown in Figure 16; the values were based on that provided in reference [7]. Heat generation within the reactor vessel was applied to the side of the heavy water tank (structure 1061) and within the coolant. The heat generation for these was assumed to be uniformly distributed and limited to the same elevation as the fuel.

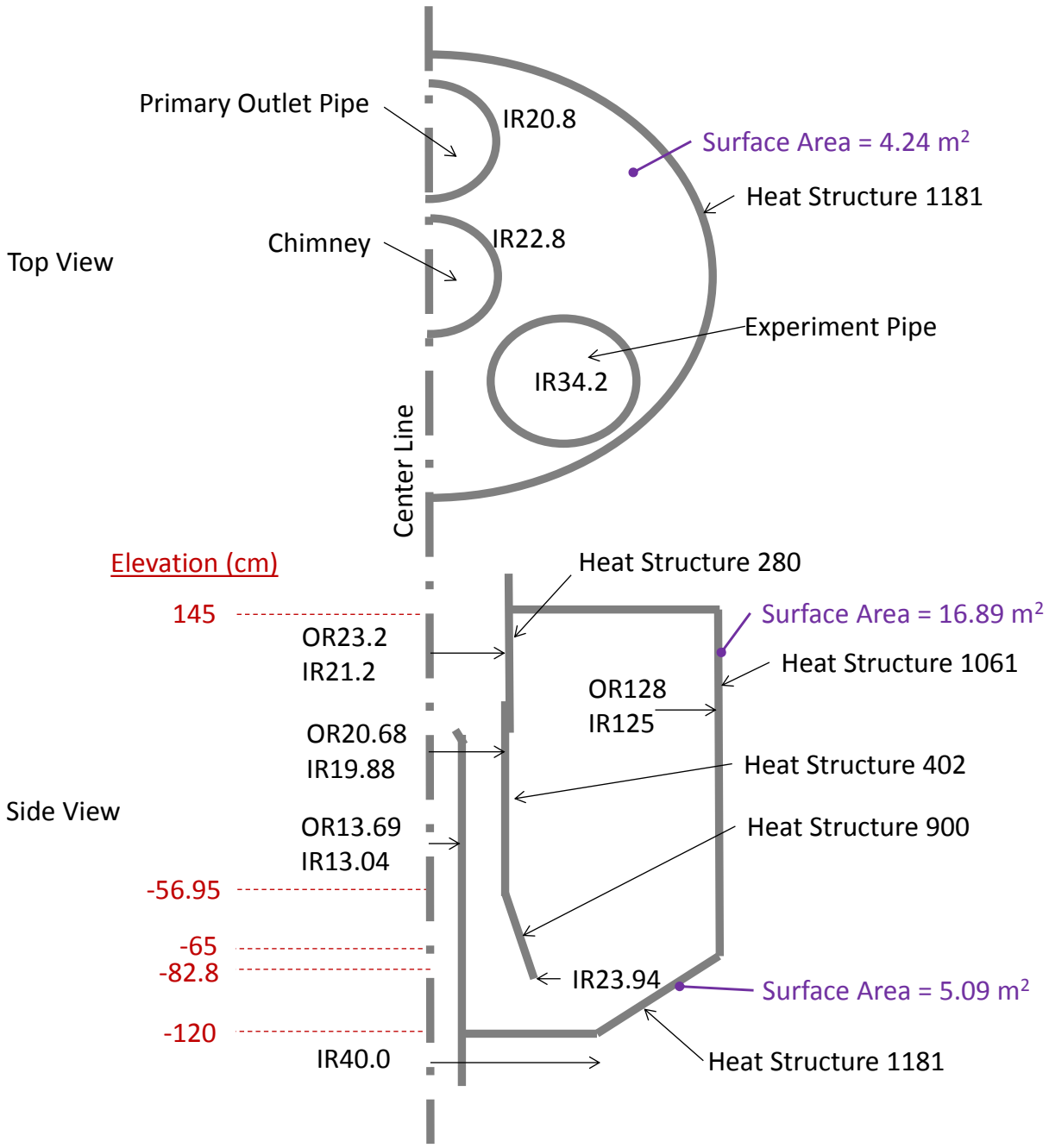

Figure 16 Conceptual drawing of RHF heavy water vessel (IR and OR = inner and outer radius, radial dimensions in cm).

2.8.4. Reactor power

Detailed axial and radial power distributions for HEU and LEU fuel at BOC (fresh core, no Xenon, "full power" conditions as described in Ref. [13], control rod 24.92 cm withdrawn) are given in Table 17 and Table 18, respectively. The methodology used to normalize MCNP tallie into power distribution is described in Ref. [13]. The power distribution given in the tables includes the four stripes for the fuel element, the control rod tubes and its coolant volumes and the reactor vessel and its coolant volumes. For the columns with a power fraction highlighted in red background color, the power fractions don't sum to 1.0 because in RELAP5 the fractions are multiplied by the power specified by the neighboring structure and not the total power generated in the coolant.

Table 17 Power distribution for HEU fuel at BOC.

HEU at BOC		Fuel				Control Rod										Reflector	
Component		Remainder	Hot Stripe #1	Hot Stripe #2	Hot Stripe #3	Volume 76	Long Ni Rod	Volume 74	Long Al rod	Volume 72	Short Ni rod	Volume 70	Short Al rod	Above Control Rod	Within Control Rod	Reflector	Vessel Wall
Heat Structure		400	410	420	430	760	760	740	740	720	720	700	700	360	740	402	1061
RELAP5 Table		9	10	11	12	13	13	14	14	15	15	16	16	17	14	18	19
Power (W)		4.26E+07	4.35E+06	3.84E+06	2.26E+06	7.61E+04	4.73E+05	6.88E+04	5.92E+04	4.09E+03	6.62E+04	3.64E+03	8.32E+03	3.38E+04	*5.12E+05*	3.69E+06	3.98E+05
Power Ratios (Axial Segment)	1					0.1019	0.6337	0.7365	0.6337	0.0309	0.5000	0.2186	0.5000		8.6453		
	2	0.0431	0.0380	0.0381	0.0561	0.0295	0.1832	0.2129	0.1832	0.0309	0.5000	0.1259	0.2880				
	3	0.0417	0.0382	0.0381	0.0540	0.0295	0.1832	0.2129	0.1832			0.0927	0.2120	0.0833		0.0417	
	4	0.0433	0.0400	0.0400	0.0538									0.0833		0.0417	0.0417
	5	0.0443	0.0412	0.0413	0.0537									0.0833		0.0417	0.0417
	6	0.0445	0.0427	0.0426	0.0498									0.0833		0.0417	0.0417
	7	0.0448	0.0448	0.0446	0.0442									0.0833		0.0417	0.0417
	8	0.0453	0.0454	0.0452	0.0442									0.0833		0.0417	0.0417
	9	0.0466	0.0471	0.0471	0.0444									0.0833		0.0417	0.0417
	10	0.0468	0.0472	0.0472	0.0445									0.0833		0.0417	0.0417
	11	0.0478	0.0483	0.0484	0.0456									0.0833		0.0417	0.0417
	12	0.0478	0.0483	0.0484	0.0456									0.0833		0.0417	0.0417
	13	0.0475	0.0480	0.0481	0.0451									0.0833		0.0417	0.0417
	14	0.0475	0.0480	0.0481	0.0451									0.0833		0.0417	0.0417
	15	0.0461	0.0466	0.0467	0.0436											0.0417	0.0417
	16	0.0457	0.0462	0.0462	0.0432											0.0417	0.0417
	17	0.0437	0.0442	0.0443	0.0410											0.0417	0.0417
	18	0.0424	0.0430	0.0431	0.0396											0.0417	0.0417
	19	0.0403	0.0411	0.0412	0.0376											0.0417	0.0417
	20	0.0377	0.0388	0.0388	0.0351											0.0417	0.0417
	21	0.0361	0.0373	0.0373	0.0333											0.0417	0.0417
	22	0.0320	0.0337	0.0336	0.0287											0.0417	0.0417
	23	0.0314	0.0332	0.0331	0.0280											0.0417	0.0417
	24	0.0272	0.0299	0.0297	0.0230											0.0417	0.0417
	25	0.0263	0.0286	0.0287	0.0207											0.0417	0.0417
	26															0.0417	0.0417
	27																0.0417

Table 18 Power distribution for LEU fuel at BOC.

LEU at BOC		Fuel				Control Rod										Reflector	
Component		Remainder	Hot Stripe #1	Hot Stripe #2	Hot Stripe #3	Volume 76	Long Ni Rod	Volume 74	Long Al rod	Volume 72	Short Ni rod	Volume 70	Short Al rod	Above Control Rod	Within Control Rod	Reflector	Vessel Wall
Heat Structure		400	410	420	430	760	760	740	740	720	720	700	700	360	740	402	1061
RELAP5 Table		9	10	11	12	13	13	14	14	15	15	16	16	17	14	18	19
Power (W)		4.21E+07	4.99E+06	4.25E+06	4.99E+06	6.65E+04	3.87E+05	6.11E+04	5.05E+04	5.12E+03	7.45E+04	4.48E+03	9.41E+03	3.32E+04	*4.52E+05*	3.18E+06	3.74E+05
Power Ratios (Axial Segment)	1					0.1088	0.6337	0.7675	0.6337	0.0344	0.5000	0.2382	0.5000		8.9556		
	2	0.0508	0.0380	0.0388	0.0695	0.0315	0.1832	0.2219	0.1832	0.0344	0.5000	0.1372	0.2880				
	3	0.0418	0.0373	0.0374	0.0579	0.0315	0.1832	0.2219	0.1832			0.1010	0.2120	0.0833		0.0417	
	4	0.0432	0.0396	0.0397	0.0563									0.0833		0.0417	0.0417
	5	0.0439	0.0406	0.0407	0.0558									0.0833		0.0417	0.0417
	6	0.0440	0.0422	0.0423	0.0498									0.0833		0.0417	0.0417
	7	0.0440	0.0438	0.0439	0.0439									0.0833		0.0417	0.0417
	8	0.0445	0.0446	0.0447	0.0436									0.0833		0.0417	0.0417
	9	0.0454	0.0464	0.0464	0.0429									0.0833		0.0417	0.0417
	10	0.0456	0.0465	0.0465	0.0430									0.0833		0.0417	0.0417
	11	0.0463	0.0474	0.0474	0.0436									0.0833		0.0417	0.0417
	12	0.0463	0.0474	0.0474	0.0436									0.0833		0.0417	0.0417
	13	0.0461	0.0472	0.0471	0.0432									0.0833		0.0417	0.0417
	14	0.0461	0.0471	0.0470	0.0432									0.0833		0.0417	0.0417
	15	0.0448	0.0460	0.0459	0.0419											0.0417	0.0417
	16	0.0444	0.0456	0.0456	0.0416											0.0417	0.0417
	17	0.0426	0.0440	0.0440	0.0397											0.0417	0.0417
	18	0.0415	0.0430	0.0428	0.0384											0.0417	0.0417
	19	0.0397	0.0413	0.0412	0.0364											0.0417	0.0417
	20	0.0371	0.0390	0.0388	0.0336											0.0417	0.0417
	21	0.0358	0.0379	0.0378	0.0319											0.0417	0.0417
	22	0.0313	0.0343	0.0342	0.0261											0.0417	0.0417
	23	0.0312	0.0342	0.0341	0.0259											0.0417	0.0417
	24	0.0281	0.0321	0.0316	0.0215											0.0417	0.0417
	25	0.0356	0.0345	0.0347	0.0269											0.0417	0.0417
	26															0.0417	0.0417
	27																0.0417

Comparisons of the power distribution used in RELAP5 and CATHARE models are shown in Figure 17 with respect to that calculated with the MCNP code. The range of axial power distribution for each of the RELAP5 heat structures (400, 410, 420, and 430) agrees well with that used in the CATHARE model. The same is true for the radial distribution which is shown as vertical lines representing the range of power density for a given stripe.

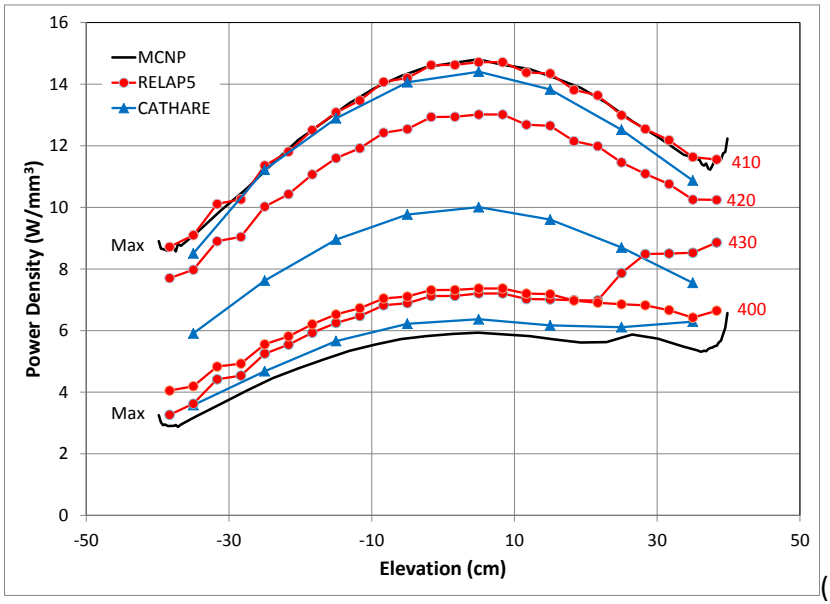

(a)

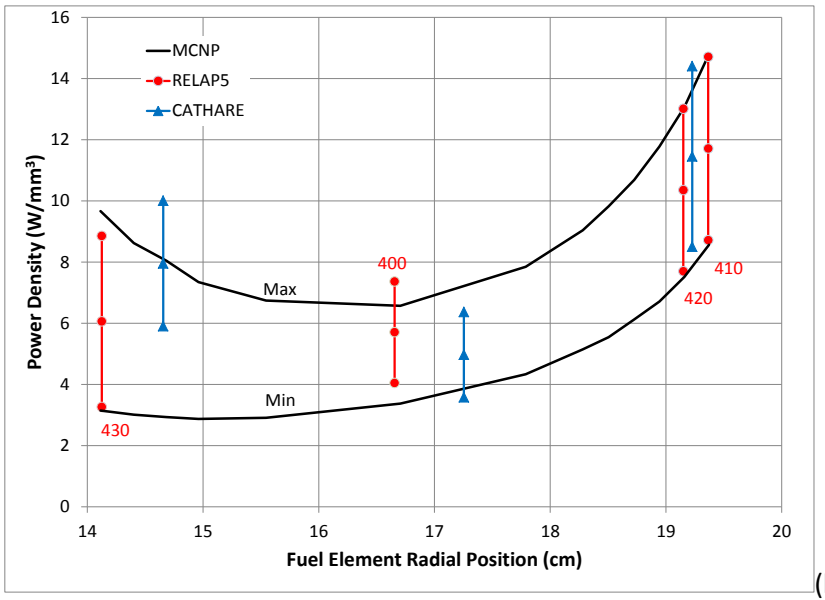

(b)

Figure 17 Comparison of axial (a) and radial (b) power density distribution in the HEU fuel element.

Table 19 shows the decay heat power curve that has been implemented in the RELAP5 model. The values were obtained from ANSI/ANS-5.1-2005 [14] for thermal fission of ^{235}U at 200 MeV/fission, 24 hours of prior operation, and includes neutron capture by fission products. The decay heat power curve has been applied to the steady state power values for each heat structure and does not take into account the redistribution of energy following a scram. Figure 18 shows that the decay heat power is initially higher than that used in CATHARE [2] but the values are quite similar after 100 s. Since it will be shown that the peak cladding temperature occurs later than 100 s, the local heat flux at the time of interest should not differ significantly between the two models.

Table 19 Decay heat power

Time after trip (s)	Decay Heat Power	Time after trip (s)	Decay Heat Power
1	5.79%	120	2.54%
1.5	5.61%	150	2.41%
2	5.45%	180	2.30%
4	5.02%	200	2.24%
6	4.73%	300	2.03%
8	4.51%	400	1.89%
10	4.34%	600	1.69%
15	4.03%	800	1.55%
20	3.81%	900	1.50%
30	3.51%	1000	1.45%
40	3.31%	1500	1.25%
60	3.01%	1800	1.16%
80	2.81%	2000	1.11%
100	2.66%	3600	0.85%

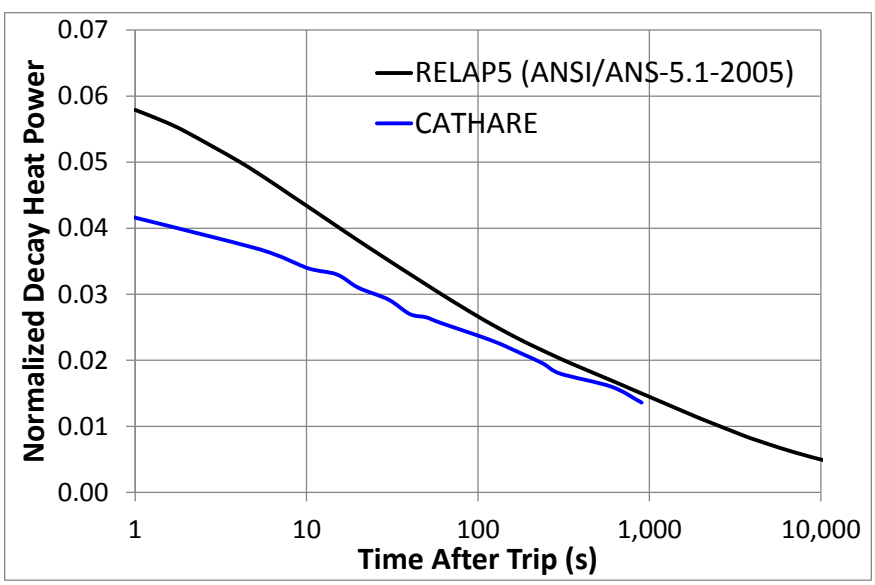

Figure 18 Comparison of the decay heat power used in RELAP5 and CATHARE.

2.9. Normal Operation at Zero Power

A set of reference reactor conditions was provided in [2] and summarized here in Table 20. As stated earlier, the pressurizer boundary condition is set to maintain a primary outlet pressure of 4 bar at volume 148(3). The total flow rate was controlled by setting the pumps velocity ratio to 0.9482. The CRAB loop flow rate (inlet and outlet) was set to 24.9 kg/s using the mass flow rate boundary conditions. These parameters are set through the use of a boundary condition and have been set to bold font in Table 20. The remaining non-bold values were RELAP5 calculated values. Results indicate that the RELAP5 model matches the target values quite well. The fact that the primary inlet and outlet pressure are correct but the pump outlet pressure, and hence the pump pressure differential, are low indicates that the pressure losses between the pump and inlet pressure measurement location are slightly underestimated. The reason for the difference could be due to the consolidation of the parallel piping and that the pressure losses due to the associated piping tees and elbows were not included. There is also a discrepancy in the anti-syphon flow rate as it is under predicted. However, it is not clear how this value was determined as there is no flow measurement made in this section of piping. It should be noted that removal of the minor loss coefficients applied to the tee's results in a flow rate very similar to reference value.

Table 20 Comparison of RELAP5 model to reference RHF parameters.

	Reference [2]		RELAP5/MOD3.3	RELAP5 Location
Mass Flow Rate	m^3/h	kg/s[8]	kg/s	Volume (node)
Primary pump	2407	735.5	**735.4**	174
CRAB pump	81.5	24.9	**24.9**	
Control rod	77.5	23.7	24.1	452
Anti-syphon	4	1.2	0.8	480
Fuel	2365	722.6	722.4	38(1)
Fuel bypass	42	12.8	13.01	34(1)
Absolute Pressure	Bar		Bar	Volume (node)
Pump inlet	4.2		4.2	166(10)
Pump outlet	16		15.6	174(1)
Primary inlet (6.1m BF1)	13.7		13.7	234(1)
Primary outlet (9.6m BC2)	4		**4.0**	148(3)
Core inlet	N/A		10.48	40(1)
Core outlet	N/A		2.67	40(6)
Pressure differential	Bar		Bar	Volume (node)
Δp fuel plate	8		7.8	40(1) – 40(6)
Δp pump	12		11.4	174(1) – 166(10)
Δp heat exchanger	1.5		1.42	190(2) – 198(1)

Further comparisons can be made for the core region by comparing the inlet and outlet core pressure to CFD simulations in Ref. [4]. The pressure losses in the core are relatively simple to determine as they only consist of frictional losses for the coolant between the fuel plates and the inlet and outlet abrupt

[8] Assuming a coolant density of 1100 kg/m^3.

area change losses. Utilizing a flow rate of 2407 m^3/h (2365 m^3/h through the fuel), the calculated pressure drop in the fuel element was 7.81 bar for RELAP5. This value is close to the value specified in reference [4] of 7.71 determined from CFD simulations (slightly lower flow rate of 2336 m^3/h). The inlet pressures were 10.48 bar and 10.91 bar for RELAP5 and CFD, respectively; the outlet pressures were 3.1 bar and 2.67 bar. Differences in the magnitudes can be attributed to the method used to obtain the boundary condition pressure in the CFD results.

A comparison to previous CATHARE model results was not attempted due to the lack of clarity in the definition of the models measurement locations.

2.10. Previous Known Issues and Resolutions

The following is a brief summary highlighting the model concerns that were raised prior to this work [1] and how they were addressed:

1. *Should the CRAB loop be modeled explicitly? If so additional data would be required (pump, heat exchanger, piping, etc.)*.

   Similar to the CATHARE model, the CRAB loop has not been included in the current version of the RELAP5 model. The section describing the CRAB loop model discusses the additional required information for it to be explicitly modeled.

2. *Should the flow coastdown in the CRAB loop be calibrated using the measured data from the 1987 LOP test?*

   The CRAB loop coast down currently utilizes the measured data from the 1987 LOP test.

3. *Confirm values that are appropriate to model the equivalent heat exchanger.*

   The heat exchanger model was developed utilizing design drawings (drawing 4C-51-P1-001) and the information provided in the SAR [3].

4. *A clear and unambiguous basis for the heavy water volume in reflector region of the tank should be developed.*

   The current reflector model does not include the structures displacing heavy water inside the tank (beam tube, cold and hot neutron sources, etc.). Based on ANL best estimate calculations, ignoring these structures results in an increased heavy water volume in the reflector region from ~10 m^3 (best estimate) to ~11 m^3 (current RELAP5 model). Further discussions are required to resolve this topic.

5. *The anti-turbulence grids representation in the RELAP5 model should be clarified*.

   The dimensions provided by RHF have been incorporated by calculating the hydraulic diameter and flow area and applying these to junction 98 (between volumes 96 and 100).

6. *For the top of the heavy water tank and the conical section below, a modeling approach must be decided.*

   The surface areas of the reactor vessel were based on the dimensions provided in Ref. [7].

7. *The core inlet and outlet pressure measurements should be used as basis for the calibration of the RELAP5 model but the location of the measurements on the cold and hot leg must be provided.*

   The location of reactor measurements has been based on the locations described in the CATAHRE documents [2] and confirmed with additional information supplied by RHF.

8. *Can the depressurization curve measured in the 1987 LOP test be used as a basis to calibrate the pressure versus time representing the pressurization pump?*

   The 1987 depressurization curve has been used in the model with the modification that the total pressures as a function of time have been slightly reduced to match the normal operating pressure of the reference conditions.

9. *A basis is needed to define the actual volume of heavy water volume within the expansion vase.*

   The volume of the expansion vase was determined from the SAR [3] and a design drawing (drawing 4C-54-P8-010) provided by the RHF team.

10. *What is the appropriate method to generate the pump coastdown curve?*

    The pump coast down flow rate method has been implemented by specifying the pumps friction torque coefficients. This was done for an upper and lower bound case to capture the uncertainty in the time that the flow rate approaches zero.

11. *What steady-state operating conditions should be used to calibrate the pump coastdown model? Cold or hot conditions? Natural circulation valves opened or closed?*

    The calibration method described in this document was for zero reactor power and the natural circulation valve were operational. This is the same conditions as the 1987 LOP test.

12. *Should the analysis use the adjusted rotational velocity to match a proposed coastdown or the measured rotational velocity from the 1987 LOP test?*

    Same as topic 10.

13. *The pump model can be calibrated to obtain adequate results for RHF while using the Westinghouse pump homologous curves. Is it necessary to further investigate the RHF pump homologous curves by comparing with the data?*

    Homologous curves for the RHF pumps have been used to model the normal operating regime. Homologous curves have not been entered for the dissipation, turbine or reverse pump regimes.

If necessary, the built in Westinghouse curves can be utilized with minor modifications to the model and would be functional for all four pump regimes.

14. *Clarify what fraction of the segments before (from CB to CP12) and after the pumps (from CP13 to C14) corresponds to the inlet and outlet piping of the pumps.*

    See topic 15.

15. *Detailed information is needed about the geometry of the pumps (flow area, length, etc.) as well as the inlet and outlet piping and how they are connected.*

    The pump dimensions have been obtained from the SAR [3].

16. *The flow areas at the top and bottom of the "conical head" of the fuel element should be clarified.*

    These dimensions have been obtained from the RHF team (see Figure 14) and incorporated into volumes 34 and 36.

17. *The number of axial nodes could be increased to 24 to model more accurately the axial power peaking at BOC and EOC in the HEU fuel element. The adequate node size to model the power peaking in the LEU fuel element could be evaluated at a later time.*

    The axial nodes of the coolant and heat structure in the core region has been based on 4 nodes in fuel region (an additional node has been used at the inlet and outlet section where there is no fuel). Comparison with 16 and 24 nodes indicated that there were no significant changes in the peak cladding temperature following a loss-of-site-power simulation. The number of nodes chosen for the final model should be discussed.

18. *The position of the control rod during the cycle will affect the power deposited in the control rod. At BOC, the tip of the control rod should be near the top of the fuel element while at EOC, it should be closer to the bottom of the fuel element. Should we have models representing the actual position of the control rod at both core states?*

    The location of the control rod in the model is currently fixed with its top at the core mid-plane. This can be updated at a later date if necessary.

19. *Discuss the geometry of the pipe junctions (tee's) and the approach to model them.*

    Tee junctions have been incorporate based on a best estimate of the information provided in the CATHARE model. The minor loss coefficients for these have been described in Appendix A.

20. *The discrepancy between RELAP5 and CATHARE at the chimney inlet needs to be clarified. However, before proceeding further, it is necessary to define a set of reference pressure at various locations in order to have a basis for RELAP5 model calibration.*

Topic 20 is no longer relevant since the simulation results are in agreement with reference conditions specified in Table 20.

21. *Similarly to the pressures, it is necessary to define a set of reference mass flow rates at various locations in order to have a basis for RELAP5 model calibration. The location of inlet and outlet flow measurements should be clarified.*

    Reference information has been obtained from SAR [3] and CATHARE documents [2] and is specified in Table 20.

22. *The resistances of the natural valves and of the anti-siphon line affect the flow redistribution during the transient. The preliminary RELAP5 modeling of these valves gives results that appear consistent with the flow patterns shown in Figures D-1 to D-3. However, more detailed information about the geometry and characteristics of these various valves is needed to model the physics of the system as close as possible.*

    The SAR [3] provides information on the valves differential opening pressure and the 1987 test data gives valve opening times and opening rate. Design drawings provided by the RHF team (see Figure 8) and description in the SAR [3] provided information on the valve areas and piping sizes.

The following are additional topics of concern that have been identified since Ref. [1] was issued:

1. Investigate the effect of the reflector heavy water volume on transient analyses or improve the reflector coolant volume description in the RELAP5 model to include the beam tube structures.
2. Clarification is required for the control rod coolant volume definitions. At first glance the control rod drawing (Figure 23.2a of the SAR) for the region above RELAP5 volume 64 seem correct, but Table 27.8 of the SAR suggests that the flow from volumes 70 and 72 should discharge into volume 62 instead of volume 78. A clear description of the logic used in modeling the sections represented by volume 64 and 66 would also be useful. These should not be significant for determining the peak cladding temperature but maybe be relevant if control rod temperatures should be included in the analyses.
3. Clarification is required for the geometry of the natural circulation pipes that connect the vessel to the chimney. The hydraulic diameter and surface area for heat transfer in CATHARE does not reflect that this component is a consolidation of the three pipes that should be similar in size to the natural circulation pipe that connects the vessel to the CRAB loop.

3. Preliminary Loss-of-Offsite-Power Simulations

Preliminary LOOP simulations were performed with the operating conditions specified in Section 2.9 for both HEU and LEU fuel at BOC conditions. After reaching steady-state conditions, the RELAP5 trip model was activated and the LOOP transient was initiated. Cases were run for both the upper and lower bound pump coast down flow rate conditions described in Section 2.3.4.

Of particular interest in these simulations are the peak cladding temperatures predicted in structure 410 (high heat flux) and the system behavior (flow magnitude and direction) near the time of flow reversal. Figure 19 to Figure 25 present the results of the simulations for each of three cases. For each group of figures, results are presented for:

- HEU fuel with the upper bound pump coast down flow rate (HEU-M2),
- HEU fuel with the lower bound pump coast down flow rate (HEU-M1), and
- LEU fuel with the lower bound pump coast down flow rate (LEU-M1).

In general, the simulation results are very similar for all three cases. The only significant difference between the three cases was due to the pump coast down flow rate and the time at which flow reversal occurred (Figure 19). The occurrence of flow reversal within the fuel element differed by about 200 s for upper and lower bound pump coastdown. While there was no data to support what the correct time at which the pump flow approaches zero and flow reversal occurs, the timing does not seem to impact the magnitude of the peak cladding temperature (Figure 20). In all cases the cladding temperature peaks to ~135°C near the time flow reversal occurs. This is very similar to the values reported in Ref. [2] for the CATHARE simulations. The bulk coolant temperature (Figure 21) within the fuel element has a similar trend as cladding temperature and momentarily peaks to ~130°C near the time flow reversal. Based on the pressure within the fuel element (Figure 22), this is above the saturation temperature of the coolant (~120°C). Plotting the heat transfer mode, as defined by RELAP5, as function of time (Figure 23) shows that sub-cooled boiling begins about 10s before flow reversal occurs. Saturated boiling occurs for the limited time (~7 s) that coolant within the fuel element is above the saturation temperature. The total void within the fuel element during this time reaches a value of ~0.4 (Figure 24). Following flow reversal, the upper ~half of heat structure 410 (highest heat flux) remains in the sub-cooled boiling regime, as indicated by the heat transfer coefficient in Figure 25, while the remainder of the fuel element is single phase convection. For heat structure 420, the upper quarter remains in the sub-cooled boiling regime following flow reversal (not shown). Heat structures 400 and 430 return to single phase heat transfer following flow reversal. The top node of heat structure 430 returns to the sub-cooled boiling regime 100 s after flow reversal and remains like this for ~700 s before returning to single phase convection.

The evolution of the thermal hydraulics within the fuel element was qualitatively similar for all cases. Figure 26 shows the following sequence of events near the time of flow reversal for the reference case HEU-M1:

Up to ~150 s after initiation of the accident the decrease in heat transfer coefficient due to decreasing flow and increase in bulk coolant temperature due to flow stagnation result in a

continual increase in cladding temperature. Following this, the onset of nucleate boiling causes an increase in the heat transfer coefficient and reduction in the temperature difference between the cladding temperature and coolant temperature. The cladding temperature stabilizes while the bulk coolant temperature continues to increase. The flow rate reaches zero near the same time that voiding in the channel begins (~165 s). The total voiding within the region of the fuel element does not exceed 40%. Oscillations in the heat transfer coefficients occur as the local heat transfer modes oscillate between sub-cooled and saturated nucleate boiling. The change in ratio of buoyant to resistive forces results in an increased rate of change in the mass flow rate as it now flows in the upward (negative) direction. The upward flow brings with it the cooler water from below the fuel element, quickly reducing the bulk coolant and cladding temperature. The oscillations in heat transfer coefficient cease as the heat transfer mode returns to single phase convection followed by a slight increase in bulk coolant and cladding temperatures. The system slowly undergoes changes as the flows in the natural circulation pipes adjust themselves to their long term flow patterns (at ~270 s). Very near this same time, sub-cooled nucleate boiling again begins in the top half of the fuel element for heat structure 410 and 420 and the top quarter of the fuel element for heat structure 430. Sub-cooled nucleate boiling continues in parts of the upper fuel element where the heat flux is relatively high.

Figure 27 shows a comparison of the RELAP5 cladding temperature simulations from above (i.e. 30°C, no discretization) with that predicted by CATHARE [2]. The steady-state temperature for CATHARE is larger partially because of the larger inlet temperature (44°C vs. 30°C). The other factor is that the CATHARE model had a coolant volume and fuel element discretized into three sections where the high heat flux structure and coolant channel were 7.9 mm wide. This results in a larger temperature rise across the high hat flux channel relative to the average coolant temperature for the fuel element. Despite these two modeling differences, the peak cladding temperatures at the time of flow reversal are quite similar. An additional RELAP5 simulation was run with an increased coolant inlet temperature of 44°C and with coolant volume 40 discretized into four separate volumes. Rather than discretize the coolant into the same three sizes that were used in CATHARE, the RELAP5 model used three coolant volumes with a width of 3 mm (same as the three hot stripe structures 410, 420, and 430). The fourth coolant channel was linked to the remaining fuel element (structures 400 and 401). Even with the higher inlet temperature and channel discretization, Figure 27 shows the magnitude of the peak cladding temperature during flow reversal does not change (RELAP5 44C, with discretization). Although, there is more chaotic behavior during flow reversal as the peak cladding temperature variations are more severe with a longer duration. Interestingly, temperature, pressure and flow oscillations also occur following flow reversal as the exit coolant temperature in the high heat flux channel remains very near the saturation temperature. Oscillations cease when the exit coolant temperature falls below the saturation temperature.

Because low pressure boiling occurs at the time of flow reversal and peak cladding temperature, a number of additional simulations were performed to investigate options included in RELAP5 to deal with the associated behaviors typically encountered:

- Activated option 5: smooth's the heat transfer coefficient using an exponential-type smoothing function ($1-e^{-t/\tau}$). The time constant is equal to the time step.
- Activated option 8, 10: Limits time step for void fraction when decreasing rapidly, limits time step so pressure does not change by more than a factor of two between time steps and eases the overfilling and over pressurization of the cell.
- Activated option 20: implements a smooth bubbly-slug transition region.
- Activated option 62: uses newly developed changes the Chen F factor in PREDNB to minimize oscillations.
- Activated option 65: changes the sub-cooled boiling model by modifying the fraction of nucleate boiling heat flux that generates vapor when the bulk liquid is sub-cooled (minimizes 'on/off' behavior associated with low-pressure/low-flow conditions).
- Removed minor loss coefficients from tee models to reduce flow resistance in natural circulation pipes.
- For pump coast down, replaced torque friction with velocity control to eliminate residual pump velocity at low flow rates.
- Increased axial resolution from 4 coolant elements within the fuel region to 16 elements.
- Run RELAP5-3D to utilize option 55 and 61. Option 55 is a collection of modeling improvements designed to minimize numerical sources of oscillation for low pressure two-phase flow simulations. Option 61 further modifies constitutive relationships to reduce numerical oscillations at low pressure, specifically for vertical stratification and interfacial heat transfer in the slug flow regime.

None of the above options had a significant effect on the simulation results or the magnitude of the peak cladding temperature. In other words, the different modeling options may have changed the details of the oscillations associated with low pressure boiling but the magnitude and duration of the peak cladding temperature remained essentially the same.

The fact that the peak cladding temperature is quite similar for all cases is due to the fact that the problem is dominated by the local conditions within the fuel element (e.g. natural convection and nucleate boiling effects). The local conditions would need to exceed the critical heat flux (CHF) in order to increase the peak cladding temperature significantly beyond its current value. A CHF ratio, or margin, can be estimated by comparing the local predicted CHF with the local heat flux of heat structure 410 (location of highest heat flux). The CHF (q''_{CHF}) was estimated with a pool boiling correlation [15] defined as:

$$q''_{CHF} = C h_{lg} \rho_g \left[\frac{\sigma g \left(\rho_l - \rho_g \right)}{\rho_g^2} \right]^{0.25}$$

where the latent heat of vaporization (h_{lg}), surface tension (σ), liquid and gas density (ρ_l, ρ_g) were determined at the saturation temperature. The saturation temperature was evaluated for both the maximum and minimum pressure associated with the pressure oscillation that occurs near the time of flow reversal to generate an upper and lower bound. The coefficient C was conservatively taken to be

0.131 and the gravity (g) was specified as 9.81 m/s^2. The heat flux for structure 410 was determined from the local peak power and surface area as a function of time. The results shown in Figure 28 for the upper and lower bound CHF ratio indicate that there is sufficient margin from CHF for the relevant flow reversal times.

Natural circulation valves are included in the RHF reactor to establish long term cooling of the core. Figure 19 shows that the natural circulation valves open 23 s after the trip for all three cases. After the natural circulation valves open, there is an abrupt drop in the flow through the fuel element. This is consistent with results seen in the pump coast down simulations (Figure 4). RELAP5 simulations predict much less flow in the natural circulation piping compared to the results predicted by CATHARE (Table 21). This difference is primarily due to the large loss coefficients applied to the Tees in the piping associated with the natural circulation valves. Removal of these coefficients from the RELAP5 model produces results that are more similar to the CATHARE results. While no flow measurements in the natural circulation piping are available from the RHF facility, the magnitude of the flow can be estimated from the magnitude in change of the mass flow rate measured at the primary piping outlet. The increase in mass flow rate resulting from opening the natural circulation valves shown in Figure 4 seems to indicate that including the minor loss coefficients for the tee junctions in RELAP5 better captures the flow diverted from the primary loop to the natural circulation piping.

Table 21 Peak mass flow rate in natural circulation pipes

	Maximum flow (kg/s)		**Long term flow (kg/s)**	
Location	**CATHARE**	**RELAP5**	**CATHARE**	**RELAP5 (800 s)**
Primary Piping	60	35	4.34	2.7
Chimney	80	32	2.9	1.8
CRAB	15	15	-1	~0

At steady-state conditions with power, Figure 29a shows the magnitude (kg/s) and direction of the coolant flow for the reference case (HEU-M1). During normal operation the natural circulation valves are closed and there is no flow through them. For the remaining figures, changes in arrow color have been used to indicate that the direction in flow has changed from the previous figure. Figure 29b shows the magnitude and direction of the coolant flow 160 s after the LOOP, just prior to flow reversal. This is well after the natural circulation valves have opened and the flow in the CRAB loop has stopped. For all other locations, the direction of flow has remained the same. The magnitudes have decreased significantly at most locations. Figure 29c shows the mass flow rate and flow direction 50 s after flow reversal (assuming flow reversal occurs at 165 s). Flow has ceased in the primary piping beyond the anti-syphon line. The flow direction has reversed at all other locations except for the anti-syphon line and the natural circulation piping connecting the inlet and outlet primary loops. For long term cooling (Figure 29d) the flow patterns remains the same except that the flow direction again reverses in the natural circulation piping of the chimney and CRAB loop.

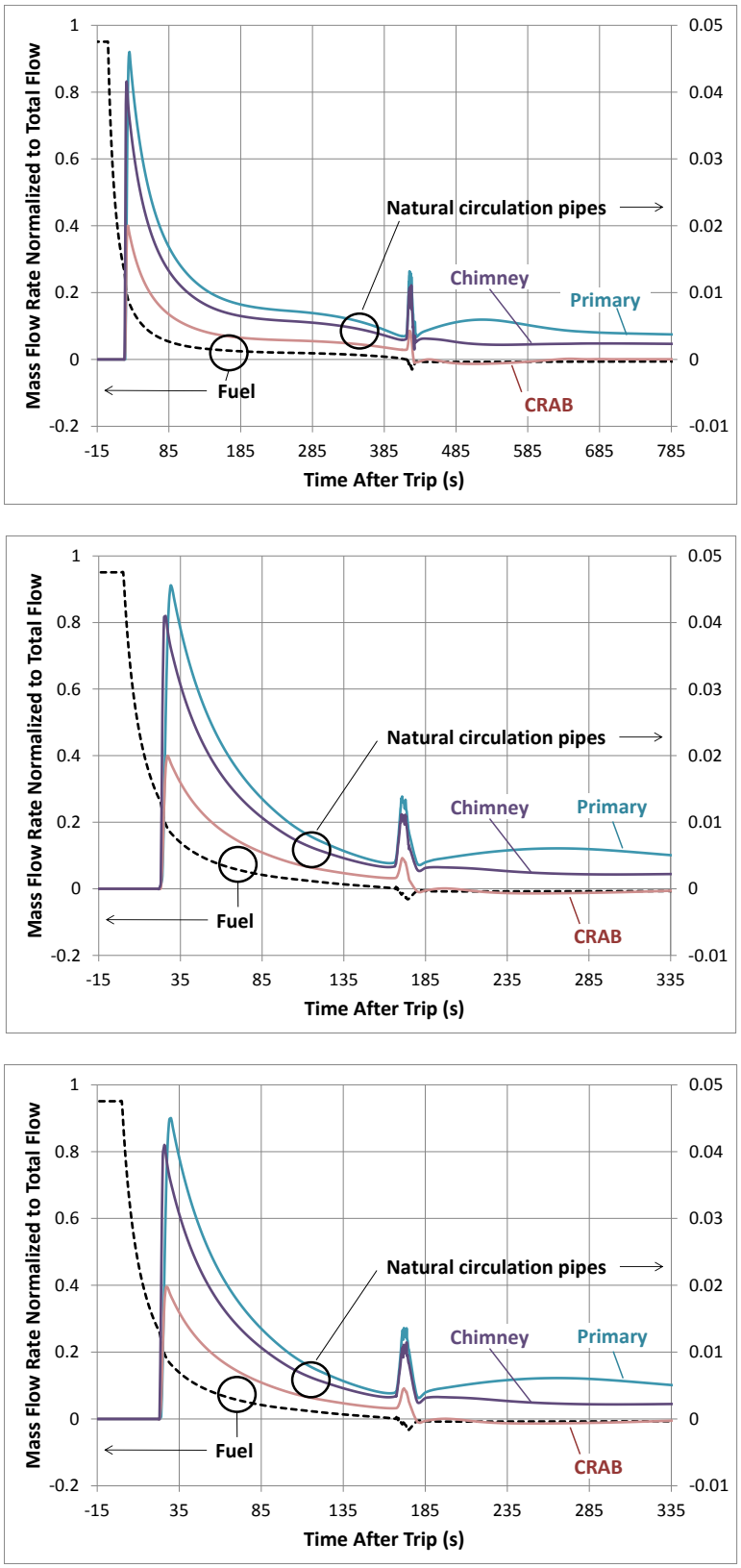

Figure 19 Normalized flow rate for fuel and natural circulation pipes. (Top: HEU-M2, Middle: HEU-M1, Bottom: LEU-M1)

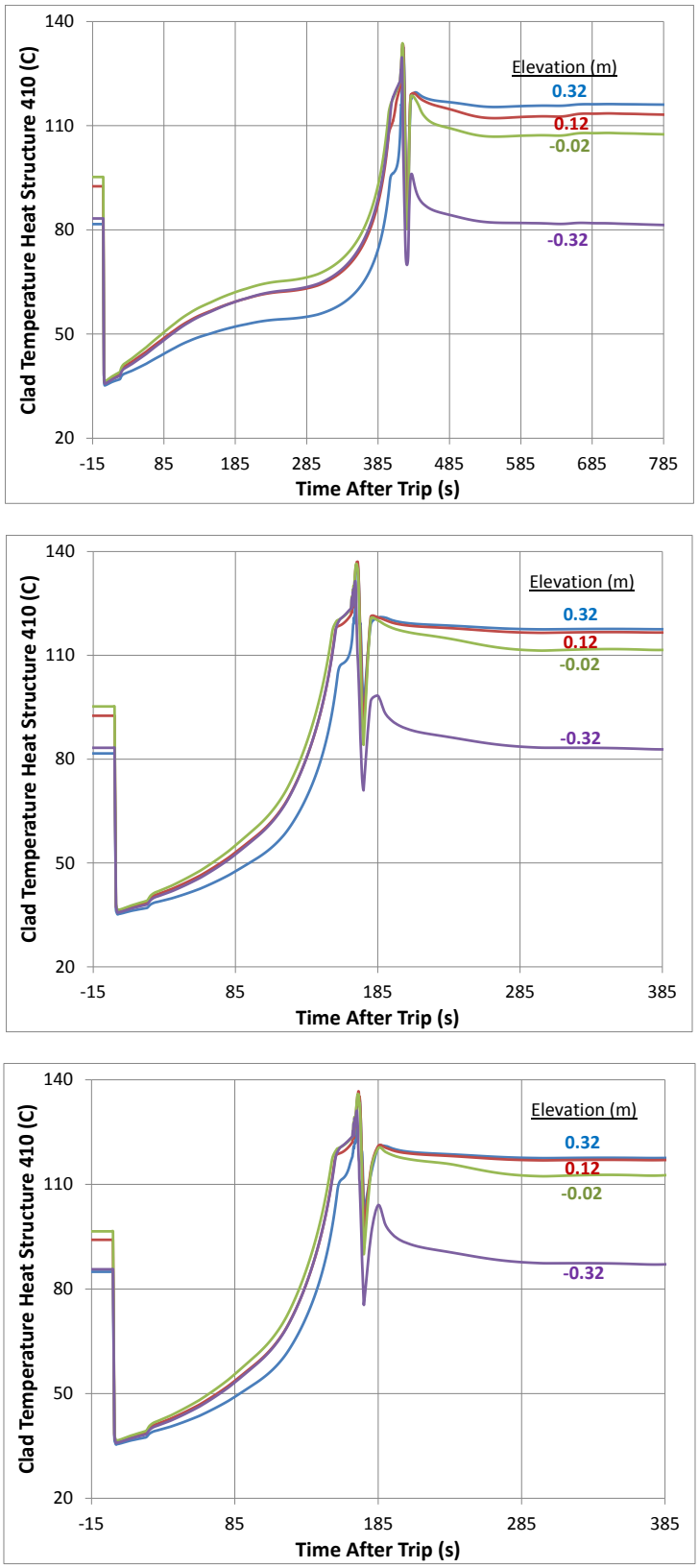

Figure 20 Cladding temperatures along the heated section of heat structure 410. Black lines with red squares are the data points extracted from the CATHARE model results. (Top: HEU-M2, Middle: HEU-M1, Bottom: LEU-M1)

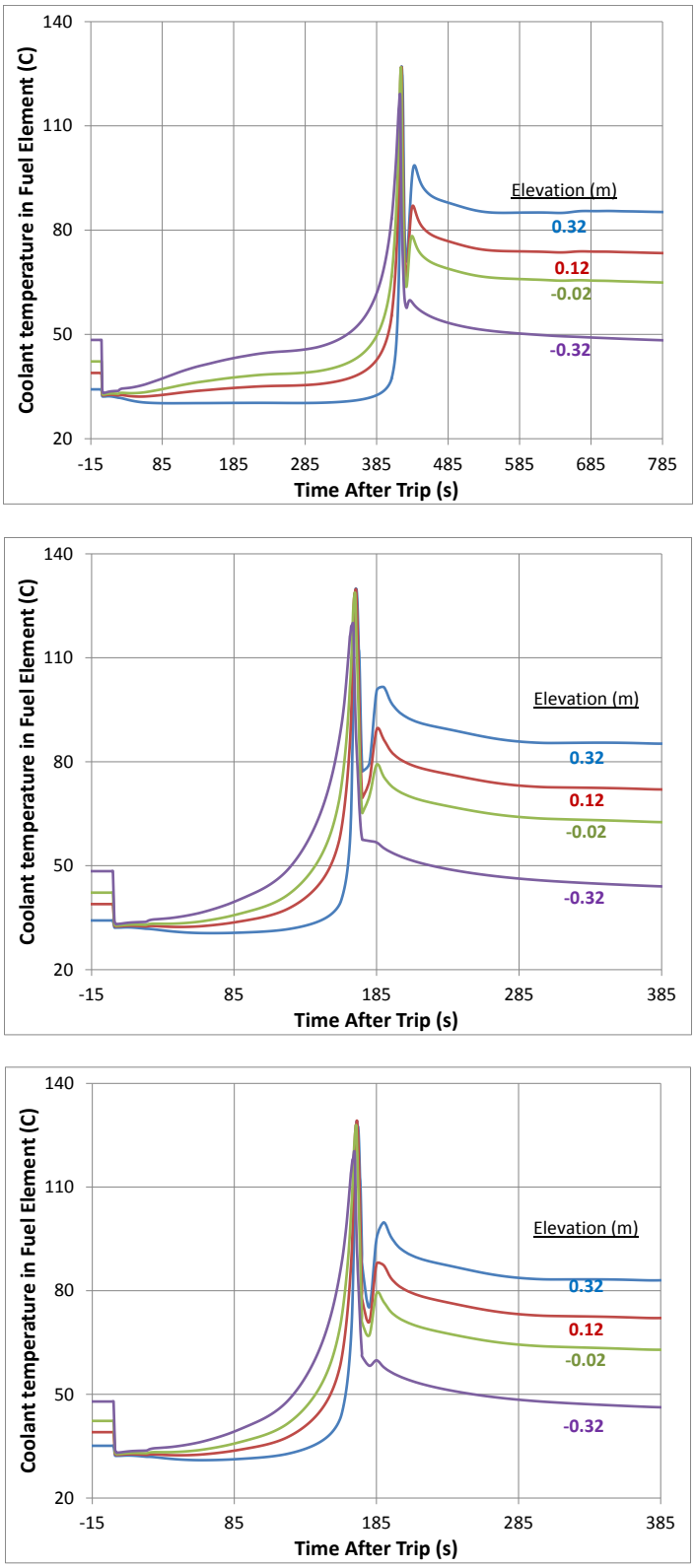

Figure 21 Bulk coolant temperatures along the fuel element. (Top: HEU-M2, Middle: HEU-M1, Bottom: LEU-M1)

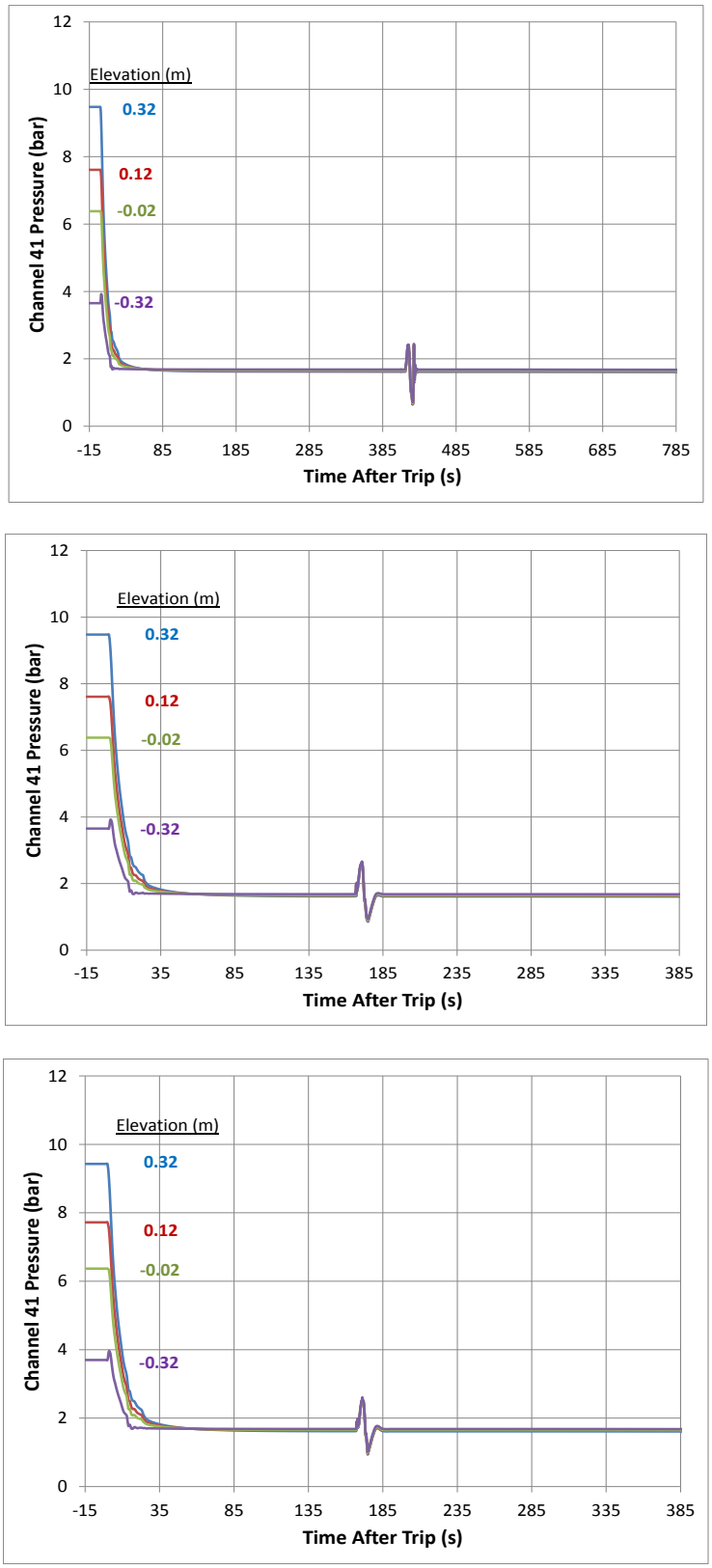

Figure 22 Pressure in fuel element. (Top: HEU-M2, Middle: HEU-M1, Bottom: LEU-M1)

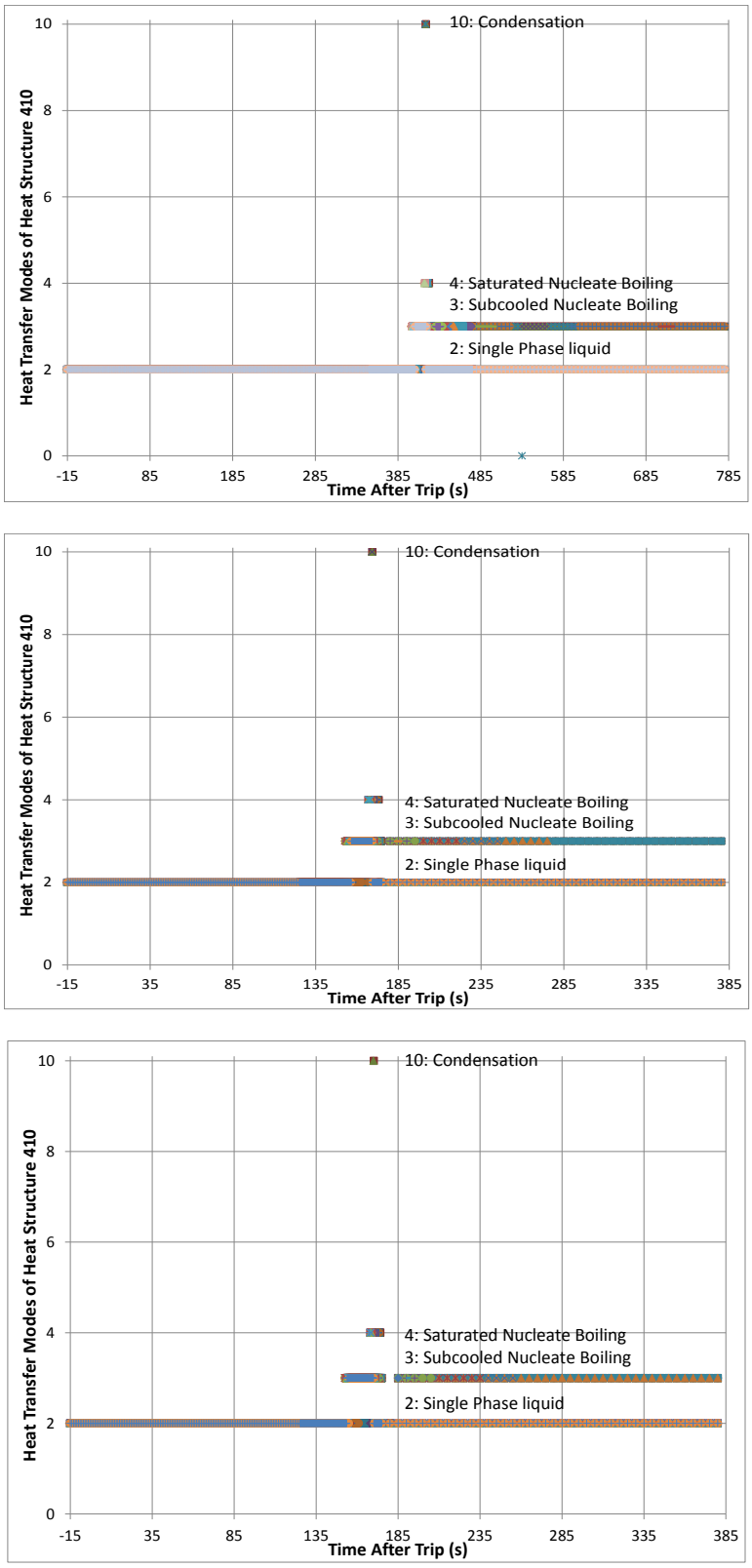

Figure 23 Heat transfer modes, as defined by RELAP5, at the surface of heat structure 410. (Top: HEU-M2, Middle: HEU-M1, Bottom: LEU-M1)

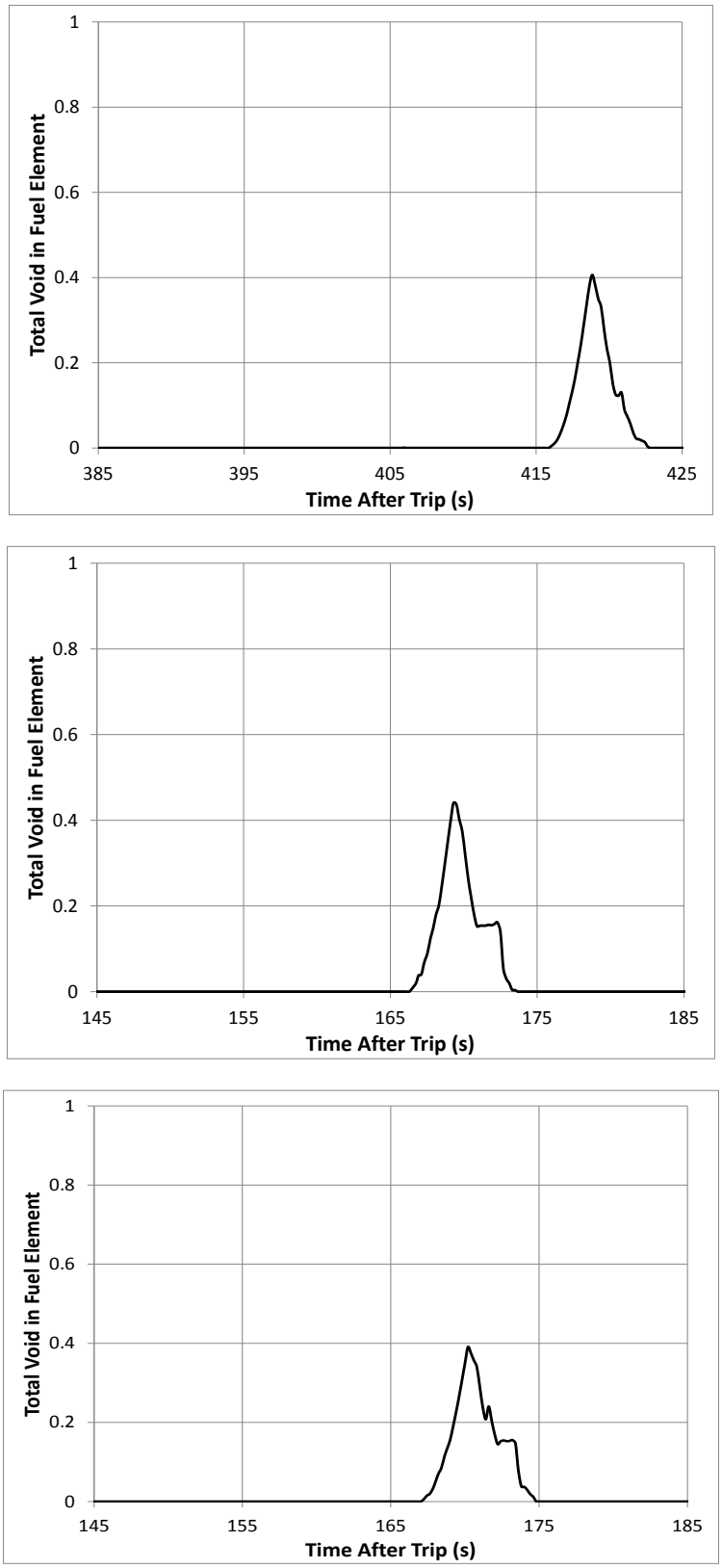

Figure 24 Void in fuel element near time of flow reversal. (Top: HEU-M2, Middle: HEU-M1, Bottom: LEU-M1)

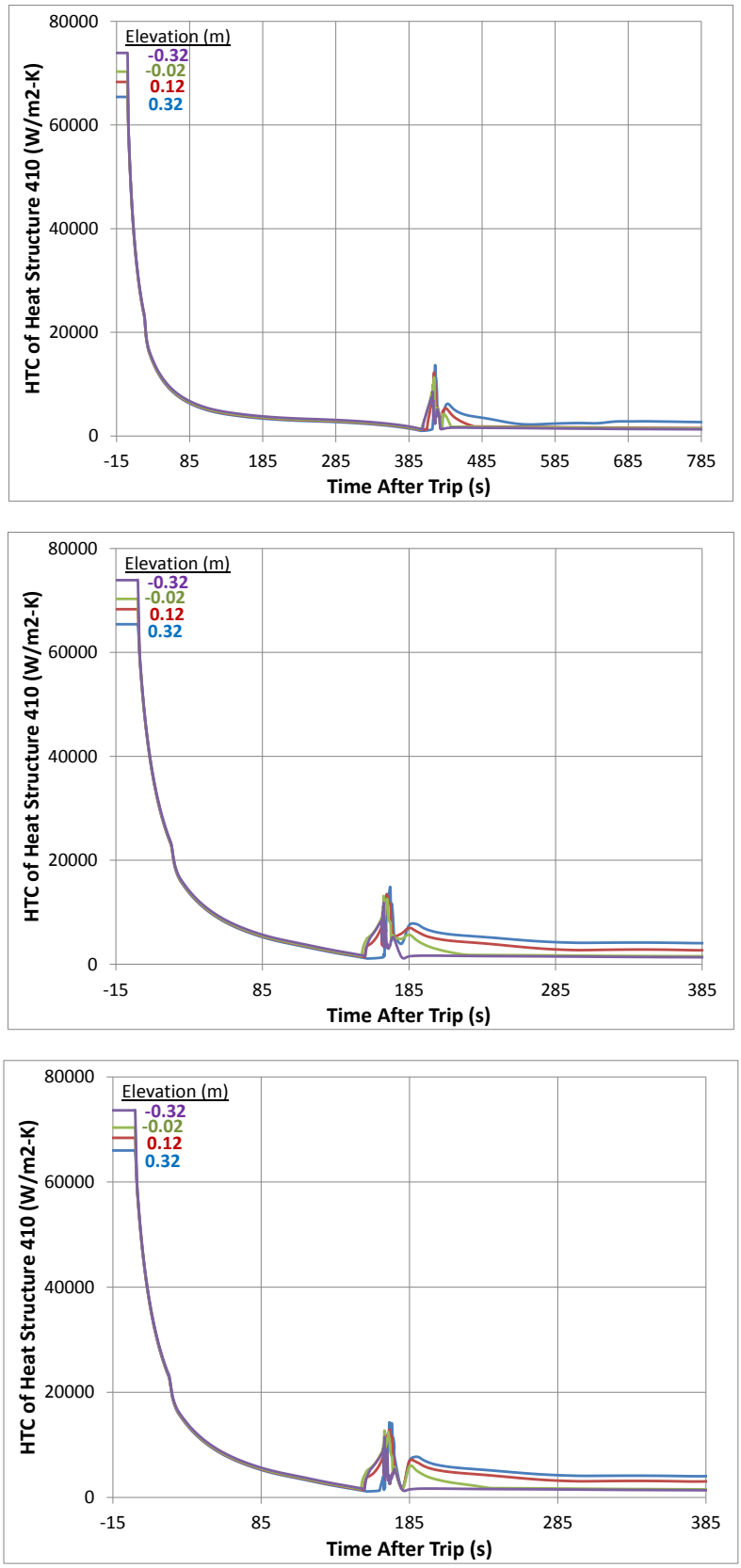

Figure 25 Heat transfer coefficient within heat structure 410. (Top: HEU-M2, Middle: HEU-M1, Bottom: LEU-M1)

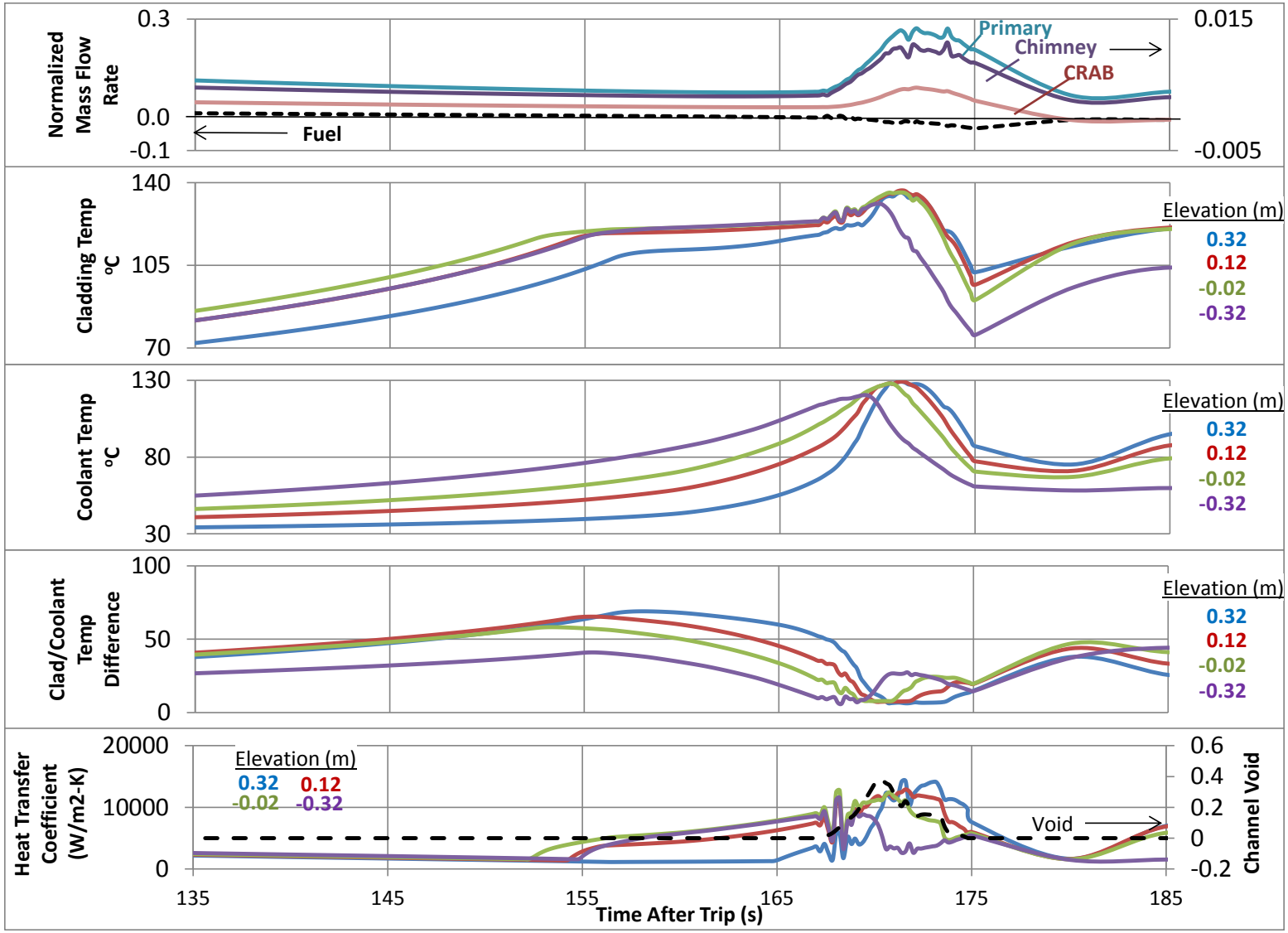

Figure 26 Comparison of thermal hydraulics near time of flow reversal for the reference case HEU-M1.

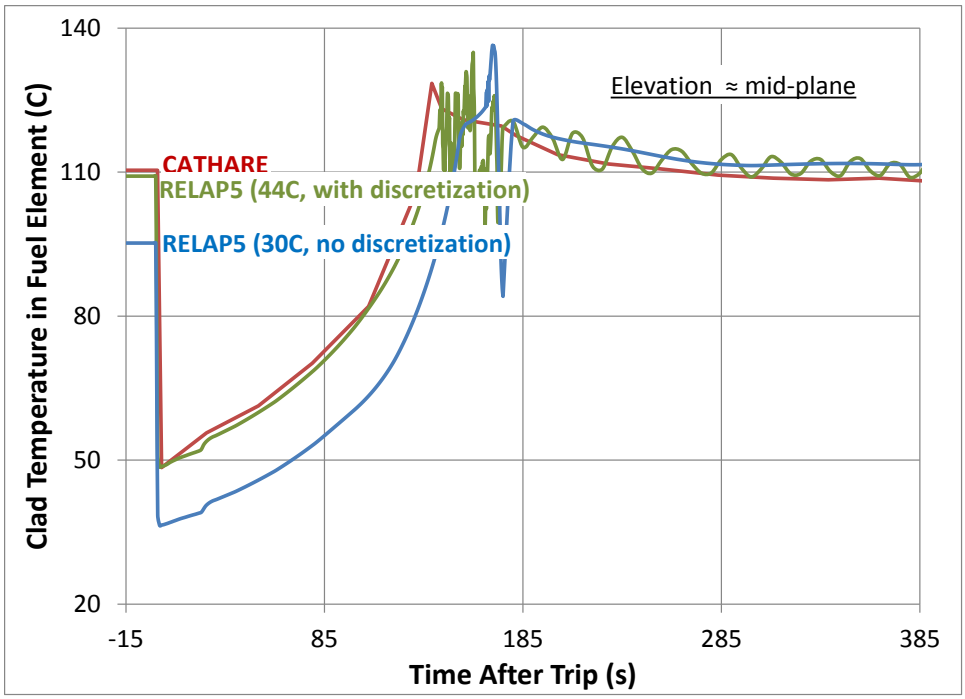

Figure 27 Comparison of the mid-plane cladding temperature for RELAP5 with and without coolant discretization and that predicted by CATHARE.

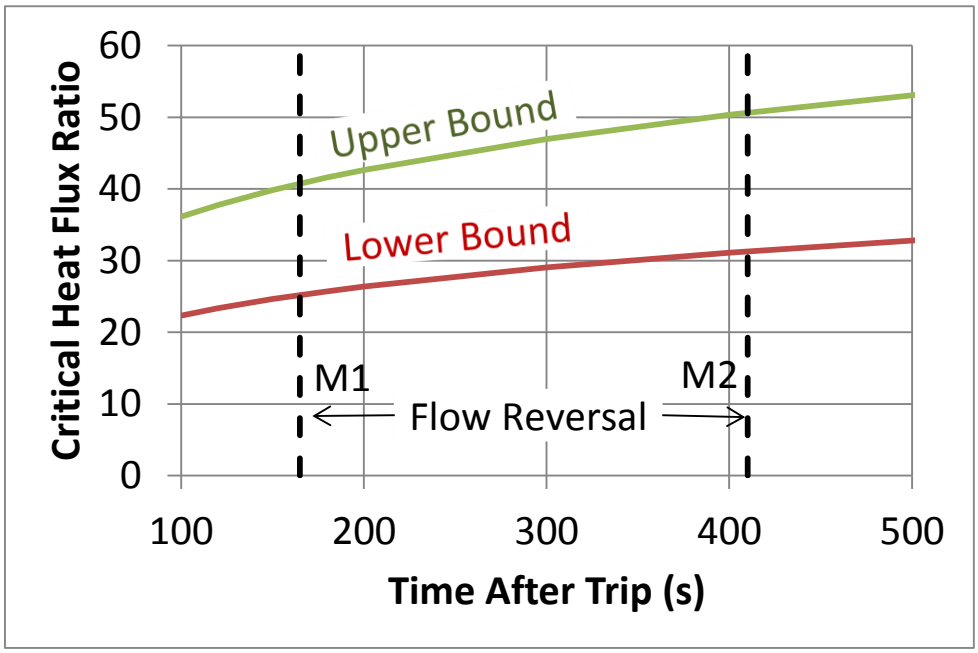

Figure 28 Critical heat flux ratio spanning the time before and after flow reversal. M1 and M2 represent the flow reversal times for each of the pump coast down curves.

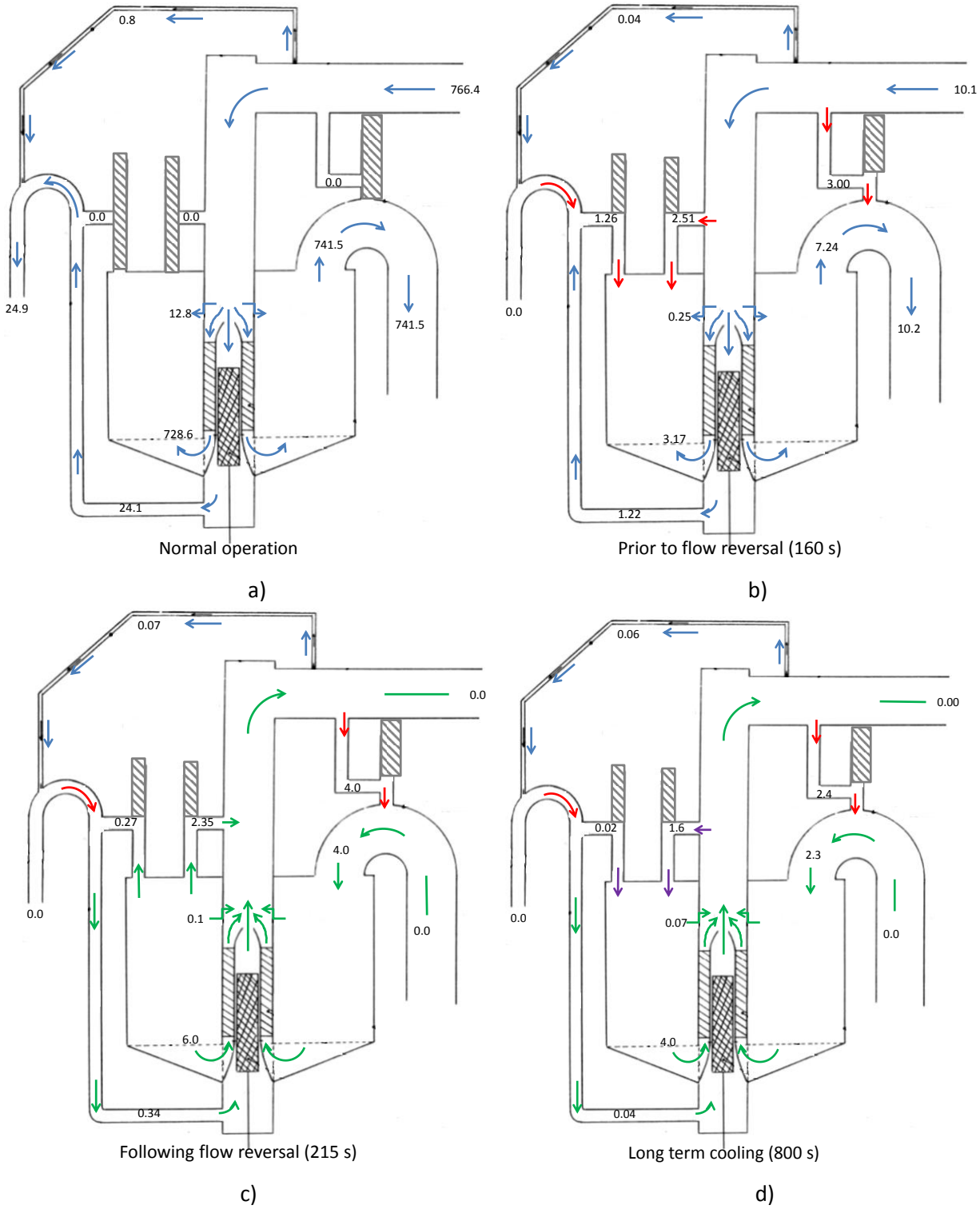

Figure 29 Magnitude (kg/s) and direction of coolant flow at various times of the transient. Arrow color is indicative of change in flow direction from previous diagram. (HEU-M1)

4. Summary and Conclusions

The purpose of this document was to describe the RELAP5 model that was developed by ANL to study transient thermal-hydraulic analyses of the RHF reactor. The model was specifically setup for LOOP accidents but can be extended to other accident scenarios with minor adjustments or additions. The model geometry was primarily based on the dimensions used to develop a model for use with the CATHARE code. The RHF safety analysis report, reactor design drawings, and other miscellaneous reports were also used to confirm data or obtain information that was otherwise not available. Lastly, preliminary work on model development had identified inconsistencies, missing information, and other areas for potential model improvement. Through discussion with RHF engineers, a majority of these issues have been resolved and incorporated into the RELAP5 model.

Calibration of the model pressures and flow rates were performed using data primarily from loss-of-flow tests performed in 1987 and information in the RHF safety analysis report. A set of nominal conditions for flow rate and pressure distribution were extracted from CATHARE documents. The RELAP5 model simulation results for nominal conditions were found to agree very well with this information.

To further test the model, preliminary simulations of a LOOP accident were performed for both HEU and LEU fuel. These results were considered preliminary since the target conditions (e.g. temperature, pressure and flow rates) for accident simulations are yet to be determined. Comparison of the RELAP5 simulation results for HEU fuel with that from previous CATHARE simulations shows good agreement for the peak cladding temperature. The RELAP5 simulation results are also very similar for LEU fuel and indicate that the conversion will not negatively impact safety for a LOOP accident. The peak cladding temperature for these simulations was found to be ~135°C and occurs near the time of flow reversal within the fuel element. The uncertainty associated with the pump coast down curve was shown to impact the flow reversal timing (a difference of ~200 s) but not the magnitude in peak cladding temperature. The peak temperature does not change significantly because in all cases it is limited by nucleate boiling.

The only significant difference between RELAP5 and CATHARE simulation results was the magnitude of the natural circulation flow in the three different natural circulation pipes. This difference was mainly due to the minor loss coefficients specified at the Tee junctions in the RELAP5 model. While data directly measuring the natural circulation flow was not available, comparison of the quantity of flow diverted from the primary piping following the opening of the natural circulation valves supported the use of the minor loss coefficients and the magnitude of natural circulation flows calculated by RELAP5.

5. Future Work

The following is a list of work that could be performed to improve the RELAP5 RHF model:

- Investigate the effect of the reflector heavy water volume on transient analyses or improve the reflector coolant volume description in the RELAP5 model to include the beam tube structures.
- Resolve the differences identified in the control rod design description given in the SAR and CATHARE model and make the appropriate changes to the RELAP5 model coolant volumes and heat structures. The control rod pressure loss and flow distribution calibration would need to be redone. This may improve the predicted control rod temperatures if they are of interest.
- Resolve the differences identified for the three natural circulation pipes that connect the chimney to the heavy water tank. Changes have been made to the current RELAP5 model relative to CATHARE and have been based on the SAR description.
- Determine the redistribution of energy following scram and apply this to the decay heat curves for each of the heat structures.

The following is a list of work that is required to perform additional transient analyses:

- Define a set of nominal reactor conditions from which to initiate the accident conditions. These will ideally take into account engineering uncertainties, tolerances and limiting operating conditions.
- Compare simulation results for both BOC and EOC conditions since the power distribution is known to change significantly. One of these should be clearly defined as the limiting case and used in further analyses.
- Analysis and discussion about the onset of flow instability since boiling is shown to occur during the transient.
- Identify the key accident scenarios that should be performed with the RELAP5 code.

References

[1] B. Dionne, A. Bergeron and C. Tzanos, Argonne National Laboratory, unpublished information, 2013.

[2] E. Pelle, "Note de réalisation du transitoire accidentel < Perte totale des alimentations électriques >," CSSI/312-1/AJ02L050/NRT/LOT4/1.0, 11/04/2003.

[3] "Réacteur à Haut Flux", INB n67, Rapport de Sureté, 2004.

[4] F. Thomas, Y. Calzavara and H. Guyon (ILL); A. Tentner and A. Bergeron (ANL), "Thermo-hydraulique d'une lame RHF," Rapport RHF n 414, February 29, 2012.

[5] "Etude du refroidissement de l'élément combustible et de la barre de pilotage du Réacteur à Haut Flux, à la suite de la perte totale des alimentations électriques," SPECIFICATION TECHNIQUE Re 3C 53 S 3001 Ind. A.

[6] Information Systems Laboratories Inc., 2003. RELAP5/Mod3.3 patch 03 Code Manual.

[7] Y. Calzavara, S. Fuard, A. Bergeron, Evaluation of measurements performed on the French High Flux Reactor (RHF), NEA/NSC/DOC(2006).

[8] B. Dionne, Y.S. Kim, and G.L. Hofman, "Thermal properties for the thermal-hydraulics analyses of the BR2 maximum nominal heat flux", ANL/RERTR/TM-11-20 Rev 0, May 23, 2011.

[9] MatWEb website, http://www.matweb.com/search/DataSheet.aspx?MatGUID=5edc39d3b0fd44efa9fdd90d049c3737&ckck=1

[10] MatWEb website, http://www.matweb.com/search/DataSheet.aspx?MatGUID=5f6bec9d37a84a77bcf295bf3653ac58

[11] hpalloy website, http://www.hpalloy.com/alloys/descriptions/NICKEL201.html

[12] I.E. Idel'chik, Handbook of hydraulic resistance, 1966.

[13] Y. Calzavara et al. "Etude Neutronique du RHF," RHF report 447, 2012.

[14] American Nuclear Society, ANSI/ANS-5.1-2005, Decay Heat Power in Light Water Reactors, April 1st, 2005.

[15] Handbook of Heat Transfer Fundamentals, 2nd Edition, by McGraw Hill.

Appendix A: Tees

The first section explicitly describe the Tee junction modeled at RELAP5 volume 134 as an example for how forward and reverse loss coefficients were determined. The second section summarizes information for all RELAP5 Tee junctions.

Tee 134 (forward loss)

Figure 30 illustrates the RELAP5 Tee for the pressurizer pipe (260) connection to the primary outlet pipe (132-136). In addition to the default setting, the y-crossflow has been activated for volume 134. All y-direction friction has been disabled and the y-length has been specified as the diameter of volume 134.

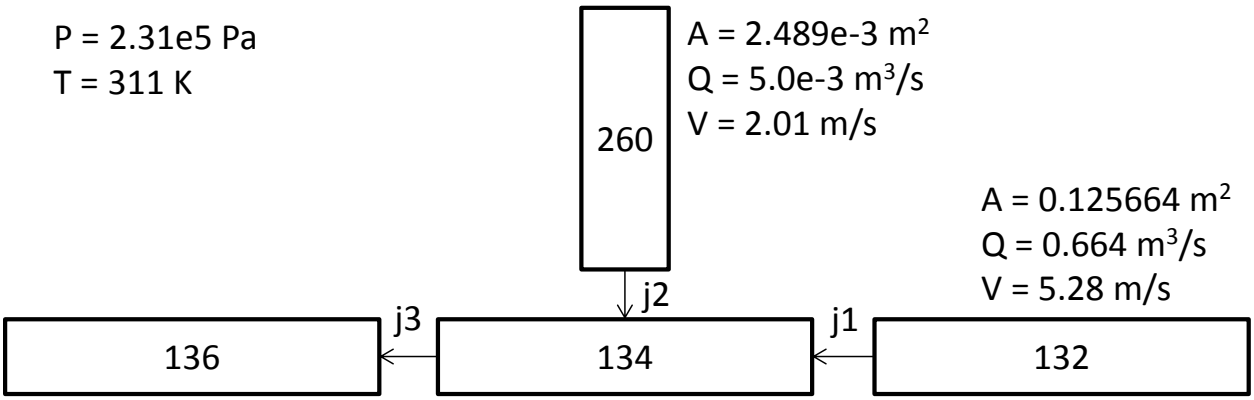

Figure 30 Tee located at junction of pressurizer and primary piping.

The forward and reverse loss coefficients have been determined by evaluating the difference in predicted loss coefficient values (Idel'chik [12) and that calculated by the RELAP5 crossflow model under typical normal operating conditions. Although the RELAP5 model utilizes a pressure boundary to replace the pressurizing effect of the pressurizer pumps, the loss coefficients were determined assuming the RHF specified pressurizer pump flow rate. Determining the RELAP5 calculated losses requires describing the momentum equations of the tee for the idealized case of steady-state, single-phase, no gravity, and no friction. The momentum equation at junction 2 is:

$$P_{260} + \frac{1}{2}\rho\left(V_{260,x}^2 + difvfx_{260,x}\right) = P_{134} + \frac{1}{2}\rho\left(V_{134,y}^2 + difvfx_{134,y}\right) + \frac{1}{2}\rho K_{junction} V_{j2}^2$$

The momentum equation at junction 3 is:

$$P_{134} + \frac{1}{2}\rho\left(V_{134,x}^2 + difvfx_{134,x}\right) = P_{136} + \frac{1}{2}\rho\left(V_{136,x}^2 + difvfx_{136,x}\right)$$

The pressure of volume 134 can be eliminated to obtain an equation resembling the Bernoulli equation:

$$P_{260} + \frac{1}{2}\rho V_{260,x}^2$$
$$= P_{136} + \frac{1}{2}\rho V_{136,x}^2 + \frac{1}{2}\rho\left(difvfx_{136,x} - difvfx_{260,x}\right)$$
$$+ \frac{1}{2}\rho\left[\left(V_{134,y}^2 + difvfx_{134,y}\right) - \left(V_{134,x}^2 + difvfx_{134,x}\right)\right] + \frac{1}{2}\rho K_{junction} V_{j2}^2$$

In this form, the RELAP5 calculated loss coefficients can be defined as

$$K_1 = \frac{\left(difvfx_{136,x} - difvfx_{260,x}\right)}{V_{j2}^2}$$

$$K_2 = \frac{\left[\left(V_{134,y}^2 + difvfx_{134,y}\right) - \left(V_{134,x}^2 + difvfx_{134,x}\right)\right]}{V_{j2}^2}$$

where they are related to the Idle'chik loss coefficient by:

$$K_{Idelchik} = K_1 + K_2 + K_{junction}$$

The *difvf* terms are an artificial viscosity defined by:

$$difvfx_{\#,x} = V_{\#,x}\left[\frac{1}{2}\left(V_{in,x} + V_{out,x}\right) - V_{\#,x}\right] + \frac{1}{2}\left|V_{\#,x}\right|\left(V_{in,x} - V_{out,x}\right)$$

The $difvfx_{136,x}$, $difvfx_{260,x}$ and $difvfx_{134,y}$ terms are zero since the inlet, outlet and mean velocities are identical. Only the $difvfx_{134,x}$ representing the junction volume is non-zero. The mean velocity in the y-direction is determined by the RELAP5 definitions of length and area in the cross flow model. If the user does not select the cross flow model but makes a cross flow connection, the default values are used with the y-direction friction enabled. Thus, the user must activate the cross flow model and de-activate the y-direction friction. By default, the y-direction length is based on the x-direction diameter. This then fixes the y-direction area since the volume is conserved in both directions. The mean velocity in the y-direction is then determined by the branch velocity times the ratio of y-direction area and branch area (conservation of mass). For this example we find that:

$$K_1 = \frac{\left(difvfx_{136,x} - difvfx_{260,x}\right)}{V_{j2}^2} = 0$$

$$K_2 = \frac{\left[(-7.96e^{-2})^2 - ((5.3)^2 - 0.106)\right]}{(2.01)^2} = -6.925$$

The target loss term for a converging tee can be determined from Idelchik table 7-7:

$$K_{Idelchik} = A\left[1 + \left(\frac{V_{260}}{V_{136}}\right)^2 - 2\left(1 - \frac{Q_{260}}{Q_{136}}\right)\right] = -0.842$$

These results are then used to determine the addition loss factor ($K_{junction}$) required to achieve the target Idel'chik loss value in the RELAP5 simulation:

$$K_{junction} = K_{Idelchik} - K_1 - K_2 = -0.842 - 0 + 6.925 = 6.083$$

Tee 134 (reverse)

The same procedure as described above can be used to determine the reverse loss coefficient for a diverging tee (the pressurizer flow rate has been reversed) with a few minor changes. The RELAP5 loss coefficients K_1 and K_2 are unchanged except for the terms 136 have been replaced with 132:

$$K_1 = 0$$

$$K_2 = \frac{[((7.96e^{-2})^2 - 0) - (5.3^2 + 0.106)]}{2.01^2} = -6.977$$

The loss term for a diverging tee was determined from Idel'chik Table 7-21:

$$K_{Idelchik} = A'\left[1 + \left(\frac{V_{260}}{V_{132}}\right)^2 - 2\frac{V_{260}}{V_{132}}cos(\theta)\right] = 1.145$$

Combining the above terms the additional loss coefficient required in RELAP5 is:

$$K_{junction} = K_{Idelchik} - K_1 - K_2 = 1.145 - 0 + 6.977 = 8.122$$

RELAP5 tee's

Table 22 summarizes the properties of each tee and the calculation results used to obtain the loss coefficients. The same process described in the previous section was used for determining the loss coefficients for the tee junction at volume 250. The remaining tee junctions are only active when the natural circulation valves open. Because each of the branch and channel flows change with time and the Idle'chik loss coefficients are dependent on flow and velocity ratios, preliminary simulation results were reviewed to determine a representative flow rate distribution.

Tee 24 results indicated that the mass flow rate in the branch remained relatively close to one half the value in the strait both before and after flow reversal. The channel velocity remained less than 0.1 m/s for prior to and following flow reversal in the core. These values result in quite a large pressure loss for both forward and reverse values. This is a diverging tee except for the brief period when flow reversal occurs.

Tee 462 is symmetrical tee in which the majority of the flow comes from the control rod from the first 400 s of the transient. The calculations were performed at the limit of all flow coming from one branch and results in a forward and reverse loss coefficient of 1.84.

Tee 132 remains a converging tee throughout the transient with branch mass flow rate being 0.25 times the channel flow rate prior to flow reversal (240 s) and approximately this value for as long as 275 seconds. After this the ratio quickly approaches one. A ratio of 0.25 was used for the calculations. A velocity of 0.27 m/s was chosen as the reference velocity of the channel.

Tee 248 behaved similar to tee 132 (within the same natural circulation piping). A velocity in the channel of 0.75 m/s was chosen since this is the value just prior to flow reversal in the core.

Table 22 Tee parameters for RELAP5 model (NC = valves are activated in the case of natural circulation)

Tee#	134	250	24 (NC)	462 (NC)	132 (NC)	248 (NC)
Connected cell parameters						
Branch Area (m^2)	2.49E-03	2.01E-04	1.51E-02	5.03E-03	0.015394	0.015394
Y velocity (m/s)	2.01	-5.53E+00	-7.02E-01	-2.00E+0	5.51E-01	-2.04E+0
Junction cell parameters						
X length (m)	0.2	0.2	0.436	0.2	0.2	0.1545
X area (m^2)	0.125664	0.125664	0.141196	5.03E-03	0.125664	0.125664
Volume (m^3)	0.0251328	0.025133	0.061561	0.001005	0.025133	0.019415
X diameter (m)	0.40000047	0.4	0.424	0.08	0.4	0.4
X velocity in (small, m/s)	5.28	5.311784	0.075	0	0.2025	1
X velocity out (large, m/s)	5.32	5.320626	0.15	2.00E+00	2.70E-01	7.50E-01
Y length (m)	0.40000047	0.4	0.424	0.08	0.4	0.4
Y Area (m^2)	0.06283193	0.062832	0.145192	0.012566	0.062832	0.048538
X mean velocity (m/s)	5.3	5.316205	0.1125	1	0.23625	0.875
Converging Tee Results						
X DIFVFX (m^2/s^2)	-0.106	-0.0235	-0.00422	-1	-0.00797	0.109375
Y MEAN VELOCITY (m/s)	-7.96E-02	1.77E-02	7.29E-02	8.00E-01	-1.35E-01	6.47E-01
K2	-6.925	-0.924	-0.006		-0.098	-0.110
K_Idel'chik (7-7)	-0.842	0.076	19.917		3.665	5.738
K_Junction	6.083	1.000	19.923		3.762	5.847
Diverging Tee Results						
X DIFVFX (m^2/s^2)	0.106	0.023503	0.004219	1	0.007973	-0.10938
Y MEAN VELOCITY (m/s)	0.07962337	-0.01768	-0.07294	-0.8	0.135	-0.64725
K2	-6.977	-0.926	-0.023		-0.150	-0.057
K_Idel'chik (7-21)	1.143	2.079	22.917		5.165	8.404
K_Junction	8.120	3.005	22.94		5.315	8.461
Symmetric Tee Results						
K2				0.160		
K_Idel'chik (7-29)				2.000		
K_Junction				1.840		

Appendix B: Supporting Analyses for RELAP5 Core Model Discretization

In order to properly simulate the peak cladding temperature during normal operation and accident conditions utilizing the RELAP5 code, special consideration must be given to the discretization of the coolant and fuel element. The cladding temperature is driven by the heat flux, heat transfer coefficient and bulk coolant temperature. The fuels power density profiles shown in Figure 31 and Figure 32 are far from uniform. A "hot stripe" of the fuel plate can be separately modeled and attributed to any particular coolant volume within RELAP5, making it relatively easy to capture the heat flux component of the peak cladding temperature (assuming only outward heat flow is a reasonable assumption). Thus, it is the radial discretization of the coolant volumes that may bias cladding temperatures. The approach used to support the coolant volume discretization was based on Computational Fluid Dynamics (CFD) simulation results. As there was no data readily available, this was the approach taken to quantify coolant and clad temperature distributions and define coolant volumes within the RELAP5 model that are appropriate to the simulation of normal operation and natural convection regimes in RHF. It is assumed that this analysis is applicable to both HEU and LEU fuel.

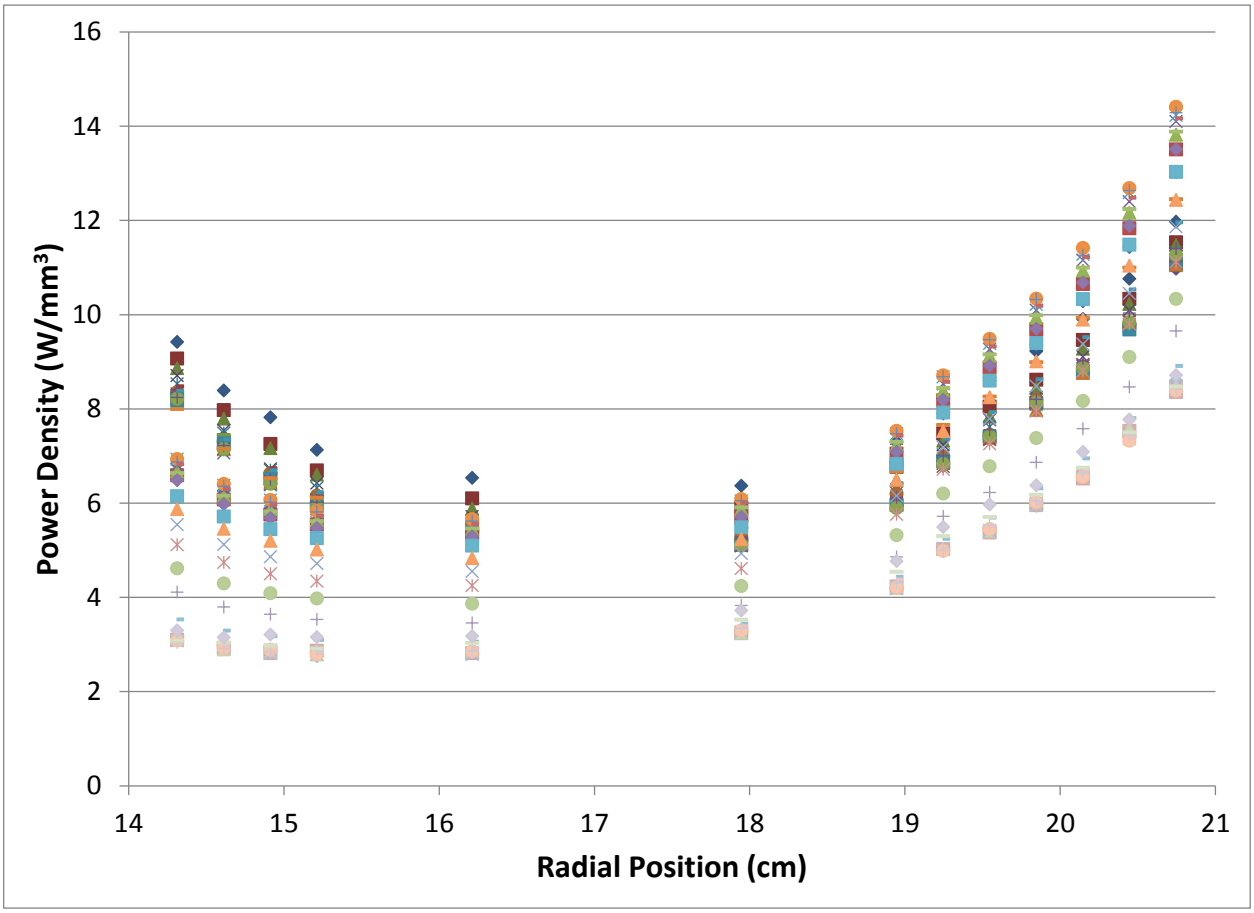

Figure 31 Power density in radial direction for each axial data set.

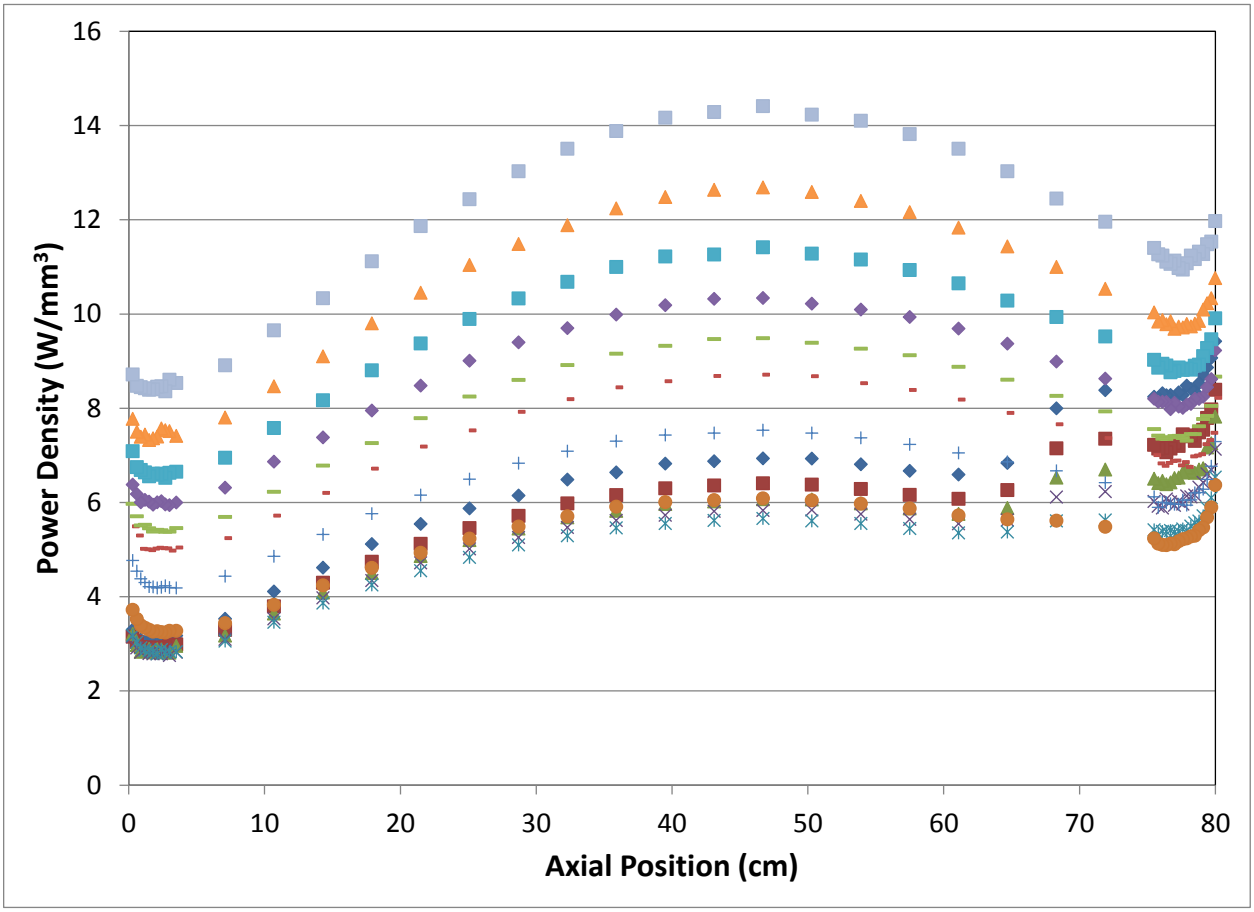

Figure 32 Power density in axial direction for each radial data set.

CFD model

The CFD code STAR CCM+ v9.02.005 was used to model a subsection of the RHF core. The first complication, or limitation, arises from the involute shape of the fuel plate. The only method available for creating an involute geometry within STAR CCM is through a spline function. This is sufficient for single volume problems but becomes difficult and time consuming for conjugate heat transfer problems where conformal geometry and meshes are desired. It was assumed that, for the purposes of these analyses, the accuracy lost from modeling the fuel element and coolant without curvature was acceptable (This error was estimated to be ~5%). Figure 33 shows the dimensions and boundary conditions for a symmetric section of a fuel plate and coolant volume, without curvature, modeled in STAR CCM. The radial dimension of the fuel plate and coolant are based on the arc length of the involute path between the concentric cylinders that bound the coolant channel (and fuel plate). The dashed lines in the figure represent boundaries used in developing a conformal mesh. For the cladding, they also represent volume boundaries. In other words, 17 volumes were used to define the cladding material. Eight of these were in the plane of the fuel and 9 in the plane between the coolant and fuel volumes. The imprint function in STAR CCM was then used to project the radial and axial boundaries onto the coolant volume, providing exact boundaries for the development of conformal mesh between the coolant and cladding interface.

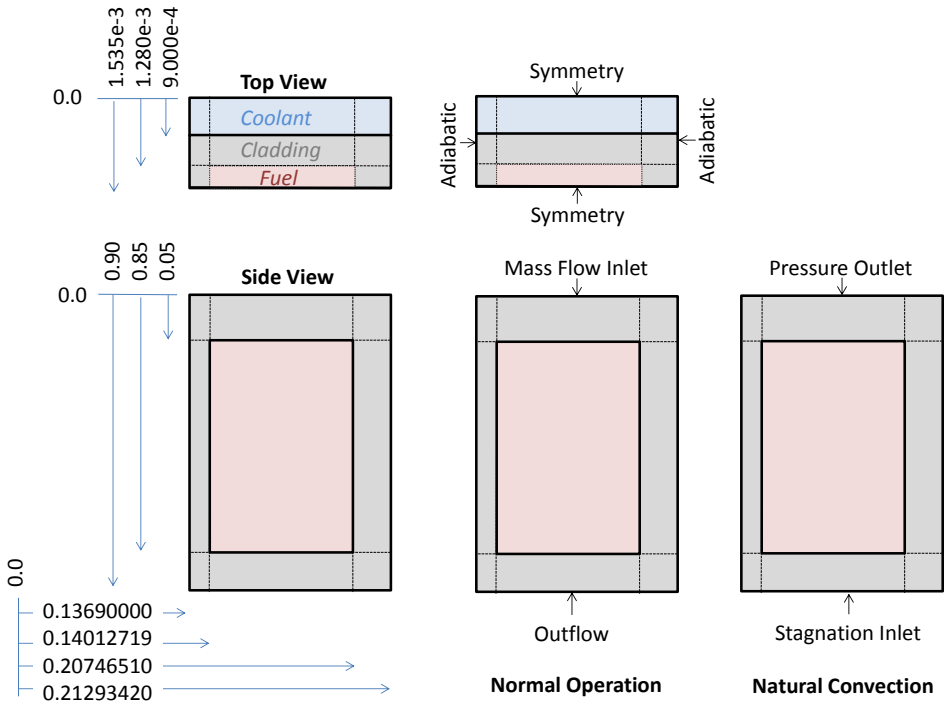

Figure 33 Geometry and boundary conditions of the fuel element and coolant. Dimensions in meters (not to scale).

Figure 34 Cross sectional view of reference volume meshing.

In total, 124564 cells were created in the reference mesh (Figure 34). Within the coolant (56620 cells), a one directional hyperbolic growth rate was selected in the direction normal to the walls. Near wall cells were sized to create near wall nodes with a non-dimensional distance ranging between y+ = 10 – 50; values that should be sufficient for a wall-function-type approach in modeling near wall physics. The radial and axial meshing in the fuel was driven by the fuels power density distribution; cell lengths in the radial and axial direction were approximately 3 mm. This discretization was maintained through the thickness of the cladding and coolant. A conformal mesh was enforced at the coolant/solid and solid/solid interfaces. The discretization in the thickness direction of the solids was set so that there were three cells within the fuel and three between the fuel and the coolant.

The meshing scheme in the fuel was based on MCNP calculations which showed that a discretization of 3 mm was required to properly resolve the power distribution. The power density distribution was applied to the fuel such that each power density value in the supplied table was associated with its corresponding cell. This was replicated for each of the three fuel cells in the thickness direction.

The Reynolds stress transport model was selected for simulating the hydraulics of the coolant since it is better suited to capturing stress-induced secondary flows associated with duct-type flows and the computational resources were readily available for the increased computational requirements of the model.

The heavy water properties were modeled with temperature dependent polynomials based on 10K increments from 290K to 400K at a pressure of 3 bar (Table 23). For values outside this temperature range, Star CCM uses the value at the range limit. The thermal physical properties for this analysis are not sensitive to the coolant pressure and should be suitable for both normal operation and natural convection simulations. The AlFeNi cladding and UAl_x-Al dispersion fuel were modeled with the temperature independent properties defined in References [6] and [8], respectively.

Table 23 Material properties used in the CFD analyses.

Material	Conductivity [W/m-K]	Density [kg/m^3]	Specific Heat [J/kg-K]	Viscosity [Pa-s]
Fuel: UAl_x-Al (BOC)	80	3580	646	
Cladding: AlFeNi	130	2702	903	
Coolant: Heavy Water (3 bar)				
290 K	0.58561	1111.1	4231	0.00136
300 K	0.59674	1098.9	4232	0.00105
310 K	0.60639	1098.9	4226	0.00084
320 K	0.61461	1098.9	4217	0.00069
330 K	0.62143	1087.0	4205	0.00058
340 K	0.62691	1087.0	4193	0.00050
350 K	0.63108	1075.3	4181	0.00043
360 K	0.63398	1075.3	4170	0.00038
370 K	0.63567	1063.8	4161	0.00034
380 K	0.63618	1052.6	4155	0.00031
390 K	0.63555	1052.6	4152	0.00028
400 K	0.63384	1041.7	4153	0.00025

For simulation of normal operation, the reference mass flow was set to 1.293 kg/s (equivalent to 724.2 kg/s through fuel element and a velocity of ~17 m/s). For natural convection simulations, the stagnation pressure was set equal to the outlet pressure and the reference density set to the value at 300 K to generate ~0 net flow at zero power conditions. Simulations were run until the residuals no longer decreased.

Three sets of calculations were performed for both normal operation and steady-state natural convection.

1. Conjugate heat transfer simulations were performed with STAR CCM to represent a best estimate of reactor core temperatures, taking into account radial and axial heat transfer in both the cladding and coolant.

2. An additional set of simulations with STAR CCM, called heat flux boundary, were performed identically to the conjugate heat transfer except that axial and radial heat transfer in the fuel and cladding was essentially mitigated by imposing an infinite thermal resistance at the coolant /clad interface outside the fuel region. This forced conditions to be nearly identical to a heat flux boundary condition at the coolant/clad interface where the heat flux distribution was proportional the power density distribution. Differences between these results and those of the conjugate heat transfer simulations provide a quantitative description of the impact heat transfer within the fuel and cladding has on the peak cladding temperature (an effect not captured in a RELAP5 model).

3. A set of 1-D calculations were performed separately to provide results equivalent to the RELAP5 methodology. For example, the radial discretization of the coolant in the CFD analysis was 22 cells (this doesn't include the unheated inner and outer edges). For the 1-D calculations, each of these cells, or columns, was treated as an isolated channel with no axial or radial heat transfer. Utilizing the local mass flow rate, inlet temperature and axial power profile from STAR CMM for each of these columns, an energy balance was used to calculate the coolant temperature axially along the channel. The axial wall temperature profile was calculated for normal operation and steady-state natural convection using the Dittus-Boelter and Churchill-Chu Nusselt correlations, respectively. Comparison of these results with those of the CFD simulations provides a quantitative estimate of the conservatism expected in the RELAP5 simulations and provides information on how best to discretize the RELAP5 coolant volumes.

Results

Figure 35 summarizes the results for each of these three different types of calculations for both normal operation (left) and steady-state natural convection (right). The first row of plots shows the radial coolant temperature distribution slightly downstream of the fuel for each set of calculations. Due to the high velocity and low coolant mixing, the results from each calculation method are quite similar. Slight differences exist near the radial extremities due to the proximity of the cooler coolant. For the natural convection case, comparison of the results shows that there are significant differences in results due to the significant amount of coolant mixing that occurs in the CFD calculations. Error bars are shown on the RELAP5 equivalent results due to the uncertainty in flow rate that would be predicted by RELAP5. The upper limit is representative of a uniform mass flow rate radially across the channel. The lower limit is based on the outlet flow rate predicted by the CFD results (mass flow distribution changes axially along the channel).

The second row of plots shows the cladding temperature and its axial distribution for the outer two channels or columns of the heated region. The heat flux boundary case produces a slightly higher

cladding temperature compared to the conjugate heat transfer case due to the higher heat flux associated with no lateral heat conduction. The difference between the heat flux boundary case and the RELAP5 equivalent at the outer cell (in the heated region) is due to thermal mixing of the coolant and the difference in heat transfer predicted by the Dittus-Boelter correlation and the CFD analysis. The later can be deduced from the fact that the heat flux and bulk coolant temperature are nearly identical at the second to last cell in the heated zone. The natural convection results appear a bit odd compared to normal operation but this is due to the low flow rate and relatively large gradient in bulk coolant temperature axially across the channel. There are also significant differences in the amount of thermal mixing, as illustrated by the differences in outlet coolant temperature.

The third row of plots shows the cladding temperature and its radial distribution at the axial location of the peak clad temperature as calculated for the conjugate heat transfer case. For normal operation the results appear similar with the exception of the differences caused by the predicted heat transfer correlation. For natural convection, the conjugate heat transfer results show that there is a cooling effect near the inner and outer edge of the heated section due to the adjacent unheated coolant. This difference was not as significant at normal operating conditions. Similarly, conduction in the fuel element also plays a role that reduces the peak cladding temperature for natural convection conditions. The RELAP5 equivalent results for natural convection are interesting in that that they reproduce cladding temperatures well for normal operating conditions but predict a significantly higher peak cladding temperature. The lack of thermal mixing in the RELAP5 simulations means the radial discretization of the coolant can have a significant effect on the predicted peak cladding temperature.

RELAP5 core discretization

Based on the results it was decided to discretize the RELAP5 heat structures into five components. Two channels (410 and 420) were based on the outer two axial stripes where the heat flux is highest. The outer structure (410) contains the highest heat flux and is considered to be the most conservative as CFD calculations predict thermal mixing and conduction in the element to be important at this location. Structure 420 has been included as a place holder in anticipation of the peak heat flux shifting to this location under other conditions. The third structure (430) is the inner stripe of the fuel element where again there is anticipation of the peak heat flux possibly shifting to this location for alternative conditions. The fourth and fifth structures (400 and 401) are for the remainder of the fuel element which contains both a heated and unheated component, respectively.

For the coolant in the core it was decided to keep this as a single channel (volume 40) linked to all of the heat structures (400, 401, 410, 420 and 430) as opposed to five coolant volumes that are linked with each of the fuel element heat structures. The impact of this discretization can be assessed by evaluating the outer heat flux stripe for the RELAP5 equivalent calculations relative to the conjugate heat transfer calculations (assumed to be the true answer). The same inlet temperature was used for each of these calculations.

For normal operating conditions, the conjugate heat transfer calculations predict a coolant outlet temperature of 326K. For an equivalent RELAP5 simulation with and without discretization, the coolant outlet temperature was 335K and 317K, respectively. This suggests that the coolant temperature will be

non-conservative by at most 9K with no channel discretization and conservative by at most 9K with channel discretization.

For natural convection, the CFD calculations predict an outlet temperature of 404K for the hot stripe. For an equivalent RELAP5 simulation with and without discretization, the coolant outlet temperature was 471K and 394K. In this case, without the effects of boiling, the outlet temperature is ~10K too low without discretization and ~67K too high with discretization.

Assuming all else is equal; the difference in coolant temperature between the equivalent RELAP5 and conjugate heat transfer calculations can be used to estimate the bias in cladding temperature. If the coolant volume is discretized, as described above, the RELAP5 calculated coolant and cladding temperature may be considered adequately conservative for normal operation but too conservative for natural convection. On the other hand, if the coolant volume is not discretized, the coolant and cladding temperature may be slightly under predicted for both normal operation and natural convection. It was decided that the reference RELAP5 model would not include discretization of the coolant volume since, although it is not conservative, it is at least not significantly different from the conjugate heat transfer calculations. A RELAP5 model that includes discretization was also created for comparison. It will be shown that the boiling also plays a significant role in LOOP simulation and that either method results in a similar peak cladding temperature. However, because mixing is not calculated between channels when discretization is used, the coolant exit temperature for the high heat flux channel is overestimated and remains at the saturation temperature for several hundred seconds following flow reversal. This leads to flow instabilities and temperature oscillations.

A third option that was not explored but could be included in future work is to optimize the coolant volume discretization by adjusting the size or number of coolant channels. However, the optimal discretization, which in itself may be difficult to define, may be different for each of the different accident scenarios that are of interest. This process would be time consuming and is likely beyond the current scope of work.

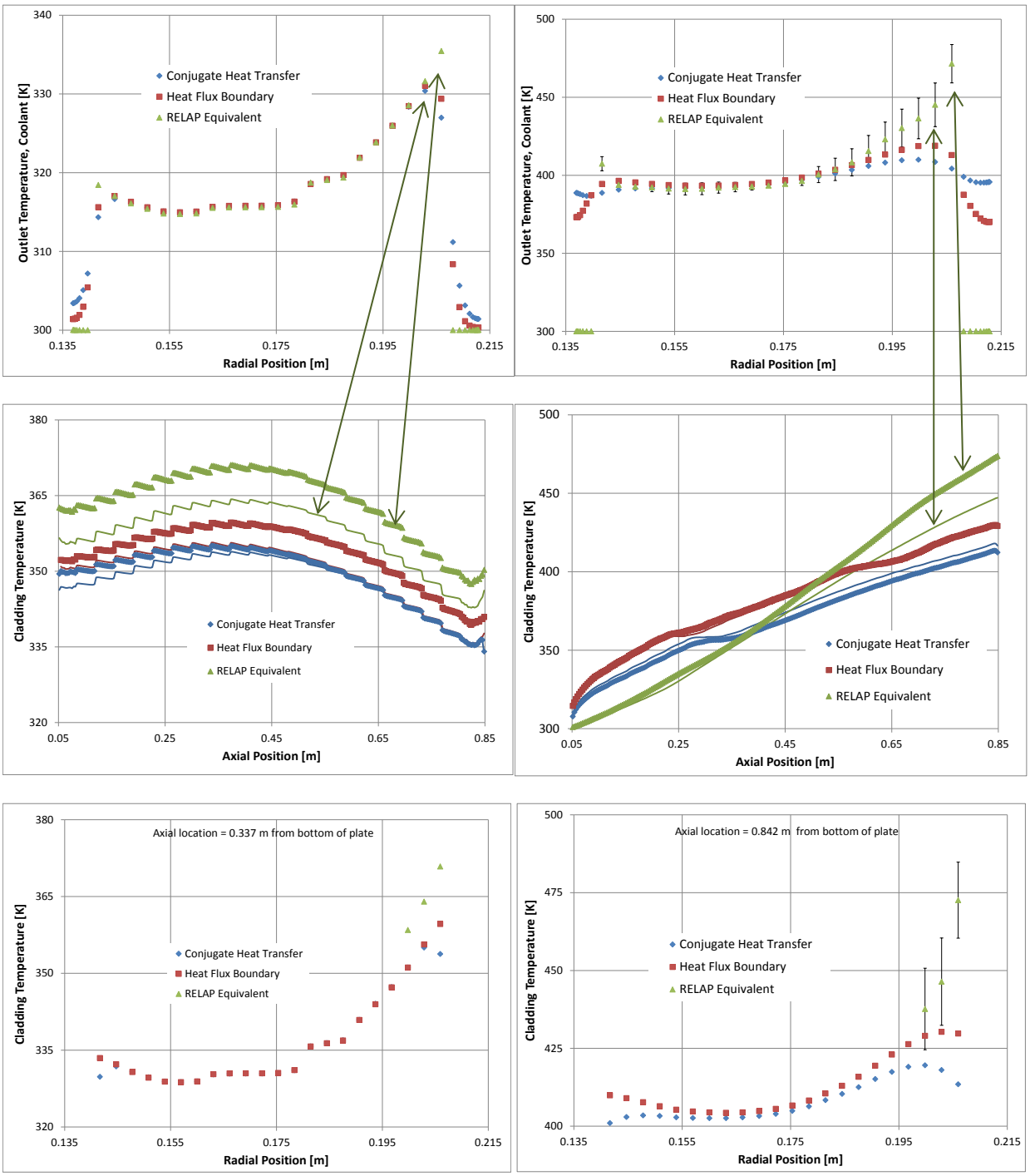

Figure 35 Left: normal operation, Right: natural convection at 3% decay power. Top: coolant temperature downstream of fuel, Middle: peak cladding temperature and axial distribution, Bottom: peak cladding temperature and radial distribution. Comparison of conjugate heat transfer including fuel element and coolant (CFD), heat flux boundary for coolant only (CFD) and expected RELAP5 results based on Churchill and Chu Nusselt correlation and no heat transfer between channels.

(This page intentionally left blank)

Nuclear Engineering Division
Argonne National Laboratory
9700 South Cass Avenue, Bldg. 208
Argonne, IL 60439-4842

www.anl.gov

Argonne National Laboratory is a U.S. Department of Energy
laboratory managed by UChicago Argonne, LLC